

On the incidence of *WISE* infrared excess among solar analog, twin and sibling stars

A. D. Costa¹, B. L. Canto Martins¹, I. C. Leão², J. E. Lima Jr¹, D. Freire da Silva ¹, D. B.
de Freitas¹, J. R. De Medeiros¹

¹Departamento de Física Teórica e Experimental, Universidade Federal do Rio Grande do
Norte, Campus Universitário, Natal, RN, Brazil, 59072-970.

²European Southern Observatory, Karl-Schwarzschild-Str. 2, 85748 Garching, Germany.

`dgerson@fisica.ufrn.br`

Received _____; accepted _____

ABSTRACT

This study presents a search for IR excess in the 3.4, 4.6, 12 and 22 μm bands in a sample of 216 targets, composed of solar sibling, twin and analog stars observed by the *WISE* mission. In general, an infrared excess suggests the existence of warm dust around a star. We detected 12 μm and/or 22 μm excesses at the 3σ level of confidence in five solar analog stars, corresponding to a frequency of 4.1 % of the entire sample of solar analogs analyzed, and in one out of 29 solar sibling candidates, confirming previous studies. The estimation of the dust properties shows that the sources with infrared excesses possess circumstellar material with temperatures that, within the uncertainties, are similar to that of the material found in the asteroid belt in our solar system. No photospheric flux excess was identified at the W1 (3.4 μm) and W2 (4.6 μm) *WISE* bands, indicating that, in the majority of stars of the present sample, no detectable dust is generated. Interestingly, among the sixty solar twin stars analyzed in this work, no *WISE* photospheric flux excess was detected. However, a null-detection excess does not necessarily indicate the absence of dust around a star because different causes, including dynamic processes and instrument limitations, can mask its presence.

Subject headings: (stars:) circumstellar matter – infrared: stars – stars: solar-type – stars: individual (HD 86087)

1. INTRODUCTION

The search for stellar infrared excesses may offer important constraints for our understanding of the nature and evolution of circumstellar dust disks, which are the most clear sign of other planetary systems. These structures may be indicative of perturbing forces, revealing the presence of planets that would otherwise remain undetected, or of other influences, including the presence of remnant gas, that may sculpt the starlight-scattering materials in these systems into ring-like morphologies (e.g.: Aumann et al. 1984; Zuckerman & Song 2004; Lagrange et al. 2009; Chen et al. 2009; Melis et al. 2013; Chen et al. 2014; Vican & Schneider 2014; Su & Rieke 2014; Meshkat et al. 2015). For instance, in the solar system zodiacal cloud, Earth has cleared out a region in its vicinity as a result of resonant tidal interactions (Dermott et al. 1994). The current literature reports debris disks composed of belts of rocks and dust around hundreds of solar-type stars (e.g., Aumann et al. 1984; Oudmaijer et al. 1992; Mannings and Barlow 1998; Chen et al. 2006; Cruz-Saenz de Miera et al. 2014; Patel et al. 2014; Chen et al. 2014), with some studies indicating that planets may be frequent in debris disks (e.g.: Morales et al. 2011; Ballering et al. 2013). Among these stars, a few dozen are also known to harbor planets (Lawler and Gladman 2012; Morales et al. 2012; Bonsor et al. 2013).

Infrared (IR) excess in main-sequence Sun-like stars is believed to result from the production of collisional dust during the final stages of planet formation, at least for relatively young stars, or produced around older stars as long as dust is liberated in higher-speed collisions (Wyatt 2008; Krivov 2010). The incidence of debris disks around main-sequence stars of spectral types A, F, G and K, based on the detection of IR excess, is reported by different authors (Habing et al. 2001; Rieke et al. 2005; Bryden et al. 2006; Chen et al. 2006; Su et al. 2006; Wyatt et al. 2007; Trilling et al. 2008; Meyer et al. 2008; Urban et al. 2012; Montesinos et al. 2016). For instance, about 20% of the nearby Sun-like

stars in the referred spectral range host dusty disks above the current detection limits (Habing et al. 2001; Trilling et al. 2008; Gáspár et al. 2013; Eiroa et al. 2013). Among the stars with detected discs, approximately 10% have ages from 10 Myr to 1 Gyr (Chen et al. 2006; Bryden et al. 2006; Meyer et al. 2008), with a clear disappearance of disks among stars older than 300 to 400 Myr (Habing et al. 1999; Wyatt 2008). More recently, Sierchio et al. (2014) have shown that among solar-type stars within the spectral type range F4 to K2, about 13% of the stars younger than 5 Gyr have dust disks, while stars most older than 5 Gyr do not.

The Wide-field Infrared Survey Explorer, *WISE*, (Wright et al. 2010), which made observations centered at wavelengths of 3.4, 4.6, 12 and 22 μm (known as the W1, W2, W3 and W4 bands, respectively), offers a unique laboratory to search for mid-IR excess in different stellar families. The 3.4-4.6 μm wavelength range is a good diagnostic of the presence of a near-IR excess, whereas the 12-22 μm range is an indicator of the presence of cooler dust. Indeed, these latter wavelengths are very sensitive to thermal emission from sources at temperatures comparable to the Earth, approximately 300 K, and to our asteroid belt and interior zodiacal cloud, approximately 150-250 K. For instance, Lawler & Gladman (2012) analysed the IR *WISE* behavior for hundreds of *Kepler* objects, including stars with confirmed planets and stars with planet candidates, and they identified 8 stars with mid-IR excesses. Morales et al. (2012) performed a analysis for a sample composed of 591 stars with confirmed planets, listed in the Extrasolar Planet Encyclopedia (Scheider et al. 2011), from which 9 stars revealed excess mid-IR emission. More recently, Cotten and Song (2016) presented a large census of infrared excess in main-sequence stars, amounting to approximately 1750 nearby and bright stars, most of which were revealed for the first time by *WISE* observations.

The primary aim of this study is to determine the incidence of mid-IR excess at

wavelengths of 3.4, 4.6, 12, and 22 μm based on homogeneous procedures for analyses of the *WISE* observations for a stellar sample composed of 216 solar sibling, twin and analog stars selected from the literature. Solar siblings refer to stars that were born simultaneously with the Sun. By definition, these stars must have a solar chemical composition considering that they essentially came from the same gas cloud and, consequently, the age of the Sun. However, solar siblings do not need to present physical parameters, such as effective temperature, mass, luminosity, surface gravity or rotation, similar to those of the Sun. Solar twins refer to stars with high-resolution, high signal-to-noise ratio (S/N) spectra that are closely identical from the spectrum of the Sun, regardless of their origin (e.g.: Cayrel de Strobel 1996; Porto de Mello & da Silva 1997; Melendez & Ramirez 2007; Ramirez et al. 2011). Solar analogs refer to those stars spectroscopically similar to the Sun, which are known to have stellar properties close to solar values (e.g.: Cayrel de Strobel 1996).

The most straightforward approach for this study is to relate the properties of debris disks around the referred stars to identify regions similar in temperature to our solar system. We revisit the search for the incidence of debris disks in 216 main-sequence stars of our sample, some of which have infrared excess already reported in the literature, searching for *WISE* infrared excess. For a solid control on the reliability of the infrared excess, we applied for each star a homogeneous diagnostic consisting of the identification of traces of IR excess in the color-color diagram, the determination of the spectral energy distributions and image inspections. The remainder of this paper is organized as follows. Section 2 presents the dataset used in our study. Section 3 discusses the method used to identify mid-IR excess and the criterion used to visually inspect the *WISE* images. Section 4 provides the main results, and the conclusions are presented in Section 5.

2. The *WISE* data and working stellar sample

WISE is a NASA infrared-wavelength astronomical space telescope that was launched in December 2009 for an all sky survey in the mid-IR with very high sensitivity (Wright et al. 2010). *WISE* has a greater sensitivity than other instruments that detect similar wavelengths. For example, its sensitivity corresponds to a factor that is approximately 1000 times greater than that obtained by the IRAS satellite (Neugebauer et al. 1984) in the 12 and 25 μm bands. Compared to the COBE satellite (Boggess et al. 1992), which made observations at 3.3 and 4.7 μm , *WISE* is approximately 500,000 times more sensitive in the 3.4 and 4.6 μm bands.

The present study is focused on searching for *WISE* infrared excess in so-called solar siblings, solar twins and solar analog stars. For this purpose, we have attempted to identify the largest set of stars defined as such in the literature. First, we selected 179 solar analogs listed by Datson et al. (2015), Chen et al. (2009) and Ramirez et al.(2012); 117 twins from Ramirez et al. (2014), Datson et al. (2015), Pasquini et al. (2008), Yana Galarza et al. (2016) and Melndez et al. (2006); 6 siblings from Ramirez et al. (2014), Liu et al. (2015) and Batista et al. (2014); and 30 siblings candidates from Liu et al. (2015). These selections correspond to a total preliminary sample of 334 stars, containing positional and photometric information, including J, H, Ks bands, from 2MASS. Nevertheless, for our study, we cross-correlated the selected sample by using 2MASS coordinates with the *WISE* all-sky data catalog, considering only those *WISE* sources located within a two arcsecond radius for which the signal-to-noise ratio is larger than 3 in all *WISE* bands, excluding stars with photometry corresponding to upper limits, as well as those with saturated fluxes. As a check of the level of saturation, for each source, we compared the *WISE* magnitudes with the saturation thresholds defined by the *AllWISE* data release (Cutri et al. 2013), according to which for sources with brightness larger than approximately 2.0, 1.5, -3.0 and

-4.0 mag in W1, W2, W3 and W4, respectively, the reliability and completeness of WISE photometric measurements degrade because there are too few non-saturated pixels available in the measurement area for reliable source extraction. Based on these criteria, the final sample consists of 121 solar analogs, 6 solar siblings, 29 solar sibling candidates, and 60 solar twins, amounting to 216 targets, composed of stars with metallicity between -0.50 and 0.45, as shown in Fig. 1. This figure shows that the peak of the distribution is located around the solar values. Based on the definition by Cutri et al. (2013), none of the stars in our final sample have saturation levels higher than acceptable, and therefore, we can consider that the observed fluxes for our sample are not overestimated. The final sample of 216 stars is listed in Table 2. This table also lists the values of the apparent magnitude V , the spectral type, effective temperature, surface gravity, metallicity and other parameters associated with the IR excess measurements, which will be defined in the next section. Fig. 2 shows the locations of 206 stars in the $\log(g)$ vs. $\log(T_{eff})$ diagram, which shows that their masses, surface gravities and effective temperatures range from approximately 1.0 to $2.0 M_{\odot}$, 3.24 to 4.8 dex and 4300 to 6900 K, respectively. These values are compatible with stars located in the main sequence stage. From the final sample of 216 stars, the 10 stars from Pasquini et al. (2008) are not represented in this figure because they do not have measured $\log(g)$ values.

2.1. *WISE* data analysis

The first diagnostic in the search for traces of IR excess was the analysis of the distribution of our final stellar working sample of 216 stars in the color-color diagram, $J - H$ versus $K - [22]$, derived from 2MASS J, H, K, and *WISE* 22 μm magnitudes, to apply the criteria established by Wu et al. (2013). According to these authors, stars with a tendency to show IR excess at 22 μm present $K - [22]$ values greater than ~ 0.22 (dashed

vertical black line in Fig. 3). The referred color-color diagram is then shown in Fig. 3, from which one observes that the large majority of stars in our sample show normal IR behavior, presenting essentially photospheric colors, i.e., $K-[22] < \sim 0.2$ are identified. However, a total of 13 stars show IR excess in the W4 band. These stars are the analogs HD 39060, HD 86087, HD 109573, HD 113766, HD 168746, HD 181296, HD 218396 and HD 224448; the twins HD 63487, HD 145927 and HD 150248; and the siblings HD 21216 and HD 168325. The 2MASS and *WISE* magnitudes used in Fig. 3 were obtained from the All *WISE* Data Release (Cutri et al. 2013).

To verify that the IR excess that emerges from the color-color diagram is actually real, we compared the observed and model-derived photospheric IR fluxes for each of the 216 stars presented in the diagram using the Virtual Observatory Spectral Analyzer (VOSA, Bayo et al. 2008). Indeed, using the VOSA procedure, we calculated the synthetic photometry in a given filter set and then performed a χ^2 minimization to determine the best fit to the data. Kurucz models (Castelli et al. 1997) were used for the fit between the observed spectral energy distributions (SEDs) and the synthetic photometry. In this procedure, we used the following ranges of stellar parameters as the input parameters: $4000 \leq T_{eff} \leq 7000$ K, $0.0 \leq \log g \leq 5.0$ and $-2.5 \leq [M/H] \leq 0.5$, covering the range of the estimated parameters for our targets.

Measurements of the *WISE* infrared excess for each source were made using the excess significance χ_λ (Beichman et al. 2006), which can be defined as

$$\chi_\lambda \equiv \frac{F_\lambda^{obs} - F_\lambda^{phot}}{\sqrt{\sigma_{obs}^2 + \sigma_{cal}^2}}, \quad (1)$$

where F_λ^{obs} is the observed flux value in the [3.4], [4.6], [12] or [22] bands; F_λ^{phot} is the theoretical photospheric flux value at the same wavelength computed from the photospheric modeling; σ_{obs} represents the errors at F_λ^{obs} ; and σ_{cal} are the absolute calibration

uncertainties of the *WISE* estimated at 2.4, 2.8, 4.5 and 5.7 percent in the [3.4], [4.5], [12] and [22] bands, respectively (see the Explanatory Supplement to the *WISE* Preliminary Data Release Products by Jarret et al. (2011)). The errors in the photospheric theoretical fluxes corresponding to the fit performed using VOSA are considered insignificant and were not used (Ribas et al. 2012). The distribution histograms of χ_λ values for the four *WISE* bands are shown in Fig. 4. The means and standard deviations from Gaussian fits (red solid curves) are 0.23 and 0.45, 0.72 and 0.94, -0.38 and 0.23, and 0.86 and 0.53 for the W1, W2, W3 and W4 bands, respectively. The negative average of χ_λ for the W3 band reflects the larger passband of W3 than the others (Wright et al. 2010; Cotten and Song 2016). Indeed, Wright et al. (2010) describes the inflight discrepancy found between red and blue sources that implies that the coolest stars will have an observed W3 flux that is fainter than the theoretical photospheric flux value, that is, a negative significance of excess.

We consider sources with an apparent significant excess as those for which $\chi_\lambda \geq 3.0$ (Su et al. 2006) in one or more of 3.4, 4.6, 12, or 22 μm bands, which corresponds to at least 3σ significance of deviation from the expected photospheric value ($\chi_\lambda = 0$). By applying this criterion, we find that 14 of the 216 stars present infrared excess in one or more *WISE* bands: At W4, HD 21216, HD 39060, HD 86087, HD 109573, HD 113766, HD 168325, HD 168746, HD 181296 and HD 218396, and all of these stars also show traces of infrared excess based on the criteria of Wu et al. (2013); at W3, HD 39060, HD 109573 and HD 113766; at W2, HD 11131, HD 96423, HD 113766 and HD 150248; and at W1, HD 6470 and HD 168746.

The stars with an apparent excess from the SEDs at W1, HD 6470 and HD 168746, and at W2, HD 11131, HD 96423 and HD 150248, were disregarded from our sample of sources considered to have an acceptable excess level. Indeed, these stars present flux ratios ($F_{12}^{obs}/F_{12}^{phot}$) close to 1, which are very low compared to those presented by stars that

exhibit significant infrared excesses at $22\ \mu\text{m}$, which are approximately 1.8. In the W2 band, the stars present an excess ratio that is more important, but according to the *WISE* Team (Cutri et al. 2012), there is an overestimation in the brightness of the $4.6\ \mu\text{m}$ band, and the bias can reach nearly 1 mag. Stars with apparent excess in bands W1 and W2 exhibit saturated pixels fractions ranging from 8% to about 50%, significantly higher than the saturated level of stars with detections in W3 and W4 which presents a range level of saturated pixels of 0.0 to 0.8%. Moreover, the overestimation of W2 magnitudes applies at most to saturated objects. The overestimation by up to 1 mag applies to objects with $W2 \sim 3$ mag, and it is smaller for stars with $3.5 < W2 < 6.5$ magnitudes. For instance, the 5 stars in our sample showing an apparent excess in W1 (HD 6470, HD 168746) and W2 (HD 11131, HD 96423, HD 150248) have W2 magnitudes between 4.8 and 7.4.

For the stars HD 150248, HD 63487, HD 145927 and HD 22448, their locations in the color-color diagram (see Fig. 3) also suggest a slight IR excess in the $22\ \mu\text{m}$ band. Despite this result, the estimated values of χ_{22} for HD 150248, HD 63487, HD 145927 and HD 22448 of 0.373, 1.090, 2.148 and 2.023, respectively, do not show confidence levels higher than 3σ , which represents the acceptable level of IR excess in our study. The SEDs for the referred stars whose IR excess were disregarded are shown in Fig. 9, presented in the online material.

2.2. *WISE* image inspection

Because different factors such as artifacts, background galaxies and other fundamental problems can contaminate the IR excesses observed in stars, we have applied a third diagnostic to define which stars with IR excess traces revealed from the color-color diagram and from the SEDs have a reliable *WISE* IR excess. In this sense, we inspected the *WISE*

images for all the stars, which were downloaded from the IRSA¹ archive, for the $1'.4 \times 1'.4$ regions surrounding each star in all *WISE* bands. The inspection is based on the following criteria:

- PSF (Point Spread Function): Check whether the photocenter of the band in which the excess is found appears to be a bona fide point source or an extended PSF.
- Offsets: Check whether the photocenter position changes in the band in which excess is found compared to its position in all *WISE* bands.
- Condition confusion flag (ccf): Check whether the photometry and/or position of a source may be contaminated or biased due to image artifact (Cutri et al. 2013). The available artifact flags are diffraction spikes (orange dots), scattered light halos (green squares) and optical ghosts (pink diamonds), as described by IRSA.

Figure 5 shows some examples of stars with excesses in the $22\ \mu\text{m}$ band as well as fundamental problems. A visual inspection shows that HD 168325 is a spurious detection in which no object is evident in the W3 band (middle left panel) and W4 band (middle right panel). This source suggests dust emission when viewed through the SEDs, but the visual analysis of the WISE image shows a lack of a point source in the W4 band.

Another star that presents fundamental problems in the image is HD 109573. Although it is a point source and has no indications of contamination by the background, the excess may be due to contamination by a diffraction spike from a nearby bright star on the same image in the $12\ \mu\text{m}$ band (top left panel) and by a scattered light halo surrounding a nearby bright source in the $22\ \mu\text{m}$ band (top right panel). Although HD 168746 (bottom panel) can be associated with a point source, this star displays a substantial contribution

¹<http://irsa.ipac.caltech.edu/applications/wise/>

from the background in the W4 band (bottom right panel), which may be related to the fact that this star is located near a stellar formation region. In this context, the objects with problems in the images, HD 168325, HD 109573 and HD 168746, were rejected from our final list of excess candidates. Their SEDs are shown in Fig.9, presented in the online material.

For the remaining stars, HD 21216, HD 39060, HD 86087, HD 113766, HD 181296 and HD 218396, the image examination indicates that such sources are clear detections of single isolated PSF sources without source confusion, and the centroid position is preserved in each image. The four *WISE* bands (from left to right, W1, W2, W3, and W4) for these stars are shown in Fig. 6.

2.3. Solar twins from M67 open cluster

An additional step in our search for *WISE* IR excess among solar twin stars was dedicated to the open cluster M67, one of the most important laboratory for studying stellar evolution (Burstein et al. 1986; Carraro et al. 1996). Commonly mentioned as a solar age cluster, with chemical composition very close to the solar values, M67 hosts 10 potential solar twins identified by Pasquini et al. (2008). These stars are MMJ5484, MMJ6055, MMJ6384, S770, S779, S785, S945, S966, S1041 and S1462, following the nomenclature used by the referred authors. All these stars present an apparent excess in the color-color diagram presented in Fig. 3, but one should consider such behavior with caution because *WISE* data show an upper limit for the magnitude K-[22], with a S/N ratio lower than 3 in the referred *WISE* band. The values of χ_λ , in the various *WISE* bands, for the M67 sample of stars are also listed in Tab. 2. By applying as a diagnostic the analysis in the *WISE* bands W1, W2 and W3 based on their SEDs, we find an IR excess in the W3 band, namely, in 12 μm , for the star S966. Nevertheless, the significance of the excess at 12 μm

for S966 is relatively low ($\chi_{12} = 3.8$). No traces of excess were observed from the SEDs of the remaining nine stars, MMJ5484, MMJ6055, MMJ6384, S770, S779, S785, S945, S1041 and S1462, which show essentially photospheric colors. The SEDs for the stars from M67 also are shown in the online material. Unluckily, a visual image inspection shows that S966 is a spurious detection. The visual analysis of the WISE images shows a lack of a point source in the W3 band, with a complex background characterizing the image in the referred band. Therefore, the apparent IR excess of the solar twin S966, emerging from the *WISE* W3 band, is indeed artificial. Therefore, we conclude that none of the solar twins stars in the M67 cluster have a detectable IR excess in the *WISE* bands.

3. Results and Discussion

Because IR excess reveals the presence of a circumstellar debris disk, we fitted the observed reliable excess for the stars HD 21216, HD 39060, HD 86087, HD 113766, HD 181296 and HD 218396 with a black body function (blue dashed lines in Fig. 7) to determine the color temperature, which is defined here as the disk temperature T_d . In the debris disk modeling, it is assumed that an optically thin dust is in thermal equilibrium with the stellar radiation field. Based on such a condition, the temperature of a dust grain with a defined chemical composition and size will depend only on the radial distance to the central star. The corresponding SEDs and the referred fits are presented in Fig. 7.

We estimated three fundamental disk properties, using equations 2 (Beichman et al. 2005), 3 (Backman & Paresce 1993) and 4 (Liu et al. 2014): the luminosity fraction $f_d = L_{IR}/L_*$, which is defined as the ratio of infrared luminosity from the dust to the stellar luminosity; the orbital distance of the dust or disk radius R_d ; and the disk mass M_d . In these equations, T_* is the effective temperature of the star, L_* is the stellar luminosity, $F_\lambda^d = F_\lambda^{obs} - F_\lambda^{phot}$ and $\frac{F_\lambda^d}{F_\lambda^{phot}}$ are the dust flux and fractional excess at 12 or 22 μm , respectively.

$$f_d = \frac{L_{IR}}{L_*} = kT_d^4 \frac{(\exp^{h\nu/kT_d} - 1)}{h\nu T_*^3} \frac{F_\lambda^d}{F_\lambda^{phot}} \quad (2)$$

$$R_d = \left(\frac{278}{T_d} \right)^2 \left(\frac{L_*}{L_\odot} \right)^{0.5} \quad (3)$$

$$M_d = f_d(R_d/9.12)M_\oplus \quad (4)$$

From this modeling, our small sample of solar analog stars with *WISE* IR excesses shows warm circumstellar material with disk temperatures T_d within the range of 150 to 270 K, luminosity fractions f_d from about 0.85×10^{-4} to 199×10^{-4} , disk radii R_d between 2.54 and 19.43 AU and disk masses from 1.11×10^{-4} to $4.23 \times 10^{-2} M_\oplus$, which also agree with the overall results found in the literature (e.g.: Chen et al. 2006; Cruz-Saenz de Miera et al. 2013; Chen et al. 2014). See table 1 for derived disk properties.

The stars identified to have reliable *WISE* IR excesses, i.e., HD 21216, HD 39060, HD 86087, HD 113766, HD 181296 and HD 218396, were previously studied by other authors by also using *WISE* data.

For HD 86087 and HD 113766, Chen et al. (2014) found a clear IR excess from *WISE* as well as from Spitzer/IRS observations. For HD 86087, we computed a *WISE* IR excess significance χ_{22} of 9.89 and fractional excess of 1.55. We also estimated a dust temperature of 175 K, luminosity fraction of approximately 1.77×10^{-4} , orbital distance of 19.43 AU and disk mass of $M_d = 7.3 \times 10^{-3} M_\oplus$. These characteristics suggest that this star is surrounded by warm circumstellar material with a temperature similar to our asteroid belt but located at a distance from the Sun greater than 7 times the distance of our belt. Based on the Spitzer spectrum in the range 5.5 - 35 μm , Chen et al. (2014) identified two dust components with dust temperatures of 381 K and 91 K, luminosity fractions of

approximately 3.7 and 9.5×10^{-5} , orbital distances of 3.9 and 84.8 AU and disk masses of $M_d = 2.7 \times 10^{-4} M_{moon}$ and $1.6 \times 10^{-4} M_{moon}$.

For HD 113766, we computed *WISE* IR excess significance in two bands, with $\chi_{12} = 20.0$ and $\chi_{22} = 17.0$ and fractional excesses of 11.42 and 63.11 for W3 and W4, respectively. The thermal emission from this object was well modeled with a single black body component, with a estimated dust temperature of 270 K, luminosity fraction of 199×10^{-4} , orbital distance of 4.4 AU, and disk mass of $M_d = 4.23 \times 10^{-2} M_{\oplus}$. The estimated dust temperature and disk radius from the present analyses are in agreement with the results obtained by Chen et al. (2006). Indeed, this is an expected result considering that the wavelengths observed by WISE ($4.6 - 22 \mu\text{m}$) are within the range of Spitzer observations ($5.5 - 35 \mu\text{m}$).

For HD 39060, Morales et al. (2012) identified warm dust emission at $22 \mu\text{m}$, estimating a dust temperature of approximately 199 K and a fractional excess of 22.8 . For the stars , HD 21216, HD 181296 and HD 218396, Patel et al. (2014) identified significant levels of *WISE* IR excess in the 12 and $22 \mu\text{m}$ bands and estimated disk properties. The dust temperatures, disk radii and luminosity fractions are 167 K, 3.7 AU and 4.1×10^{-4} , respectively; for HD 21216; 177 K, 11.0 AU and 2.5×10^{-4} for HD 181296 and 225 K, 3.3 AU and 0.6×10^{-4} , for HD 218396. For these four stars, we estimated dust temperatures and disk radii that are in agreement with those reported by these authors, as shown in Table 1. The disk masses listed in Table 1 ($10^{-4} - 10^{-2} M_{\oplus}$), estimated from the observed *WISE* IR excesses at 12 and/or $22 \mu\text{m}$, are reported for the first time for the considered stars. In general, for these stars, our results confirm and reinforce the indication of the presence of the previously detected circumstellar material with grain temperatures comparable to those of the grains in our asteroid belt and the interior zodiacal zone (Lawler & Gladman 2012; Morales et al. 2012).

3.1. On the dearth of *WISE* mid-IR excess among solar twin stars

Inspired by the reported incidence of debris disks around Sun-like stars, revealed by IR excess detections among F , G and K stars (Rieke et al. 2005; Bryden et al. 2006; Chen et al. 2006; Su et al. 2006; Wyatt et al. 2007; Meyer et al. 2008; Urban et al. 2012), we have searched in detail for traces of WISE excess emission among solar twin stars. Also, it is clear from different studies underlined in section 1, that the likelihood of a detectable debris disk depends strongly on stellar age, with a higher percentage of young stars harboring disks than older ones. For comparison purposes, as underlined in Sec. 1, approximately 10% of Sun-like stars, with ages from 10 Myr to 1 Gyr, have IR excesses reported in the literature (Chen et al. 2006; Bryden et al. 2006; Meyer et al. 2008). Nevertheless, the incidence of IR excess become sparse among stars older than 300 to 400 Myr (Habing et al. 1999; Wyatt 2008).

Our study shows that among the solar twin stars here analyzed, none have a statistically significant WISE IR excess compared to the predicted stellar photospheric flux. Indeed, the null detection of debris disks around solar twins stars can reflect different root-causes, including that dust disks around the referred stars become so optically thin to be undetectable, at their age, cold disks, which are detectable only at longer wavelengths, as well as disk disappearance due to stellar ages. At this point, the analyses of the age distribution for our sample of solar twin stars it is mandatory. Fig. 8 shows the age distribution for our sample of 60 solar twin stars, with ages taken from Yana Galarza et al. (2016), Ramirez et al. (2014), and Melendez et al. (2006); for stars from Datson et al. (2015) and Pasquini et al. (2008), age were taken from Holmberg et al. (2007) and Önehag et al. (2011), respectively. From the range of ages shown in Fig. 8, one observes that the large majority of stars are older than the expected age interval (300 to 400 Myr) for disks disappearance (Habing et al. 1999, Wyatt 2008). In this context, the dearth of

mid-IR excess among solar twin stars is rather in agreement with the scenario expected for main-sequence Sun-like stars in the same age range, pointing for a possible debris disk disappearance.

4. Conclusions

In this study, we analyzed the *WISE* emission flux properties of a sample of 216 main sequence stars, consisting of 121 solar analogs, 6 solar siblings, 29 solar sibling candidates, and 60 solar twins, in the search for infrared emission excess in four WISE bands (W1-3.4 μm , W2-4.6 μm , W3-12 μm , and W4-22 μm). Nine stars present excesses in the 12 and/or 22 μm bands at the 3σ level of confidence, but three were rejected after visual inspection of the WISE images because of fundamental problems (contamination by artifacts, no evident source and/or background emission).

We confirm *WISE* excess in 12 and/or 22 μm in the solar analogs HD 39060, HD 86087, HD 113766, HD 181296, and HD 218396, corresponding to 4.1% of the analyzed sample, and in the solar sibling candidate HD 21216, 1 out of 29 solar siblings candidates. The estimations of the dust properties for these stars with IR excesses are consistent with those given in the literature. For HD 113766, we confirm a *WISE* excess with a dust temperature of 270 K , which is compatible with other studies. These values strengthen the fact that these stars present warm circumstellar material with temperatures that are similar to the asteroid belt and interior zodiacal zone. The fractional dust luminosity ranges from about 0.85×10^{-4} to 199×10^{-4} , with HD 113766 presenting the highest fractional luminosity in the sample. The orbital distances of the dust disks estimated in the present work range from 2.54 to 19.43 AU. Star HD 21216 show dust disk within the solar asteroid belt region, whereas the disks of HD 39060, HD 86087, HD 113766, HD 181296 and HD 218396 are

outside the asteroid belt, reflecting probable differences in planetary systems. The present analyses reinforce that for the definition of IR excess, a visual inspection of the WISE images is mandatory to check the reliability of the mid-IR excess in the WISE bands because such excesses can be contaminated by artifacts or background emissions. For instance, the apparent IR excess associated with the stars S996, HD 109573, HD 168325 and HD 168746 are due to the presence of artifacts.

Finally, some relevant points should be highlighted. No stars having *WISE* photospheric flux excess at the W1 (3.4 μm) and W2 (4.6 μm) bands were identified, indicating that, in principle, no detectable hot dust is generated in the present stellar sample. The detection of a mid-IR excess revealed by *WISE* W3 (12 μm) and W4 (22 μm) suggests the presence of circumstellar warm material from primary dust generation. In this context, the identification of debris disks around stars similar to the Sun is extremely important because the circumstellar dust also represents a fundamental factor to show how special the Sun and the solar system are compared to other stars and other planetary systems. Interestingly, among the 60 solar twins analyzed here, no stars present *WISE* IR excess at a 3σ level of confidence. Such a finding may point to a very interesting scenario: stars with physical parameters similar to the Sun, as is the case of the solar twins, can in fact be very different from the Sun once the star and its circumstellar environment are considered. However, a null-detection excess does not necessarily indicate the absence of dust around a star. In this context, additional studies for the search of IR excess in other wavebands, including those by Spitzer and Herschel, are mandatory to confirm the present results about the dearth of debris disks around stars with physical parameters similar to the Sun.

Research activity of the Observational Astronomy Board of the Federal University of Rio Grande do Norte (UFRN) is supported by continuous grants from CNPq

and FAPERN Brazilian agencies. We also acknowledge financial support from INCT INEspaço/CNPq/MCT. ADC acknowledges a CAPES/PNPD fellowship. ICL acknowledges a CNPq/PDE fellowship. JEL and DFS acknowledge graduate fellowships from CAPES. This work is based on data products from the Wide-field Infrared Survey Explorer, a joint project of the University of California, Los Angeles, and the Jet Propulsion Laboratory/California Institute of Technology, supported by the National Aeronautics and Space Administration. This study has used the NASAs Astrophysics Data System (ADS) Abstract Service, the SIMBAD database, operated at CDS, Strasbourg, France, and data products from the Two Micron All-Sky Survey (2MASS), a joint project of the University of Massachusetts and the Infrared Processing and Analysis Center, supported by the National Aeronautics and Space Administration and the National Science Foundation. This study has used the VOSA support, developed under the Spanish Virtual Observatory project funded by the Spanish MICINN through grant AyA2011-24052. Finally, a special thanks to the anonymous referee for providing very helpful comments and suggestions that improved largely this publication.

REFERENCES

- Ahn C. P. et al., 2012, ApJS, 203, 21
- Allard, F., Homeier, D., & Freytag, B. 2012, RSPTA, 370, 2765
- Aumann, H. H., Beichman, C. A., Gillett, F. C., et al. 1984, ApJL, 278, L23
- Backman, D. E., & Paresce, F. 1993, in Protostars and Planets III, ed. E. H. Levy & J. I. Lunine (Tucson: Univ. Arizona Press), 1253
- Ballering, N. P., Rieke, G. H., Su, K. Y. L., & Montiel, E. 2013, ApJ, 775, 55
- Bayo, A., Rodrigo, C., Barrado y Navascues, D., et al. 2008, A&A, 492, 277B.
- Batista S. F. A., Adibekyan V. Z., Sousa S. G. et al. 2014, A&A, 564, A43
- Beichman, C. A., et al. 2005, ApJ, 622, 1160
- Beichman, C. A., et al. 2006, ApJ, 652, 1674
- Boggess, N. W., et al. 1992, ApJ, 397, 420
- Bonsor, A., Kennedy, G. M., Crepp, J. R., et al. 2013, MNRAS, 431, 3025
- Bryden, G., Beichman, C. A., Trilling, D. E., et al. 2006, ApJ, 636, 1098
- Burstein, D., Faber, S. M., & Gonzalez, J. J. 1986, AJ, 91, 1130
- Cayrel de Strobel, G. 1996, A&ARv, 7, 243
- Carraro, G., Girardi, L., Bressan, A., et al. 1996, A&A, 305, 849
- Castelli, F., Gratton, R. G., & Kurucz, R. L. 1997, A&A, 318, 841
- Chen, C. H., et al. 2006, ApJS, 166, 351

- Chen, C. H., Sheehan, P., Watson, D. M., et al. 2009, *ApJ*, 701, 1367
- Chen, C. H., Mittal, T., Kuchner, M., et al. 2014, *ApJS*, 211, 25
- Cotten, T. H., & Song, I. 2016, *ApJS*, 25, 15
- Cruz-Saenz de Miera, F., Chavez, M., Bertone, E., & Vega, O. 2014, *MNRAS*, 437, 391
- Cutri, R. M., Wright, E. L., Conrow, T., et al., Explanatory Supplement to the WISE All-Sky Data Release Products. Tech. rep. (2012).
- Cutri, R. M., Wright, E. L., Conrow, T., et al. 2013, *yCat*, 2328, 0
- Datson, J., Flynn, C., & Portinari, L. 2015, *A&A*, 574, A124
- Dermott S. F., Jayaraman S., Xu Y. L., Gustafson B. A. S., Liou J.-C. 1994, *Nature*, 369, 719
- Ducati J. R., 2002, CDS/ADC Collection of Electronic Catalogues, 2237, 0
- Eiroa, C., Marshall, J. P., Mora, A., et al. 2013, *A&A*, 555, A11
- Gspr A., Rieke G. H., Balog Z. 2013, *ApJ*, 768, 25
- Girard, L., Bertelli, G., & Chiosi, C. 2000, *A&A*, 141, 371
- Gray R. O., Corbally C. J., Garrison R. F., McFadden M. T., Bubar E. J., McGahee C. E., ODonoghue A. A., Knox E. R. 2006, *AJ*, 132, 161
- ESA, 1997, The Hipparcos and Tycho Catalogues, ESA SP-1200. ESA, Noordwijk
- Henden A. A., Templeton M., Terrell D., Smith T. C., Levine S., Welch D., 2016, *VizieR Online Data Catalog*, 2336
- Habing, H., Dominik, C., Jourdain de Muizon, M., et al. 1999, *Natur*, 401, 456

- Habing H. J. et al., 2001, *A&A*, 365, 545
- Hog, E., Fabricius, C., Makarov, V. V., et al. 2000, *A&A*, 355, L27
- Holmberg J., Nordstrom B., & Andersen J., 2007, *A&A*, 475, 519
- Houk N., Smith-Moore M., 1988, *Michigan Catalogue of Two-dimensional Spectral Types for the HD Stars. Volume 4*
- Houk, N., & Swift, C. 1999, in *Michigan Spectral Survey*, Ann Arbor, Dep. Astron., Univ. Michigan, Vol. 5, p. 0 (1999), Vol. 5, 0
- Jarrett, T., Cohen, M., Masci, F., et al. 2011, *ApJ*, 735, 112
- Krivov A. V., 2010, *Res. Astron. Astrophys.*, 10, 383
- Lagrange, A.-M., Kasper, M., Boccaletti, A., et al. 2009, *A&A*, 506, 927
- Lawler, S. M., & Gladman, B. 2012, *Apj*, 752, 53
- Liu, Q., Wang, T., & Jiang, P. 2014, *AJ*, 148, 3
- Liu, C., Ruchti, G., Feltzing, S., et al. 2015, *A&A*, 575, A51
- Mamajek, E. E., Meyer, M. R., & Liebert, J. 2002, *AJ*, 124, 1670
- Mannings, V., & Barlow, M. J., 1998, *ApJ*, 497, 330
- Marois, C., Macintosh, B., Barman, T. et al., 2008, *Science*, 322, 1348
- McDonald, I., Zijlstra, A. A., & Boyer, M. L. 2012, *MNRAS*, 427, 343
- Melendez, J., Dodds-Eden, K., & Robles, J. A. 2006, *ApJ*, 641, L133
- Melendez, J., & Ramirez, I. 2007, *ApJL*, 669, L89

- Melis, C., Zuckerman, B., Rhee, J. H., et al. 2013, *ApJ*, 778, 12
- Meyer, M. R., Carpenter, J. M., Mamajek, E. E., et al. 2008, *ApJ*, 673, 181
- Mermilliod, J. C. 2006, *VizieR Online Data Catalog*, 2168, 0
- Meshkat, T., Kenworthy, M. A., Reggiani, M., et al. 2015, *MNRAS*, 453, 2534
- Montesinos B. et al., 2016, *A&A*, 593, 51
- Morales, F. Y., Rieke, G. H., Werner, M. W., et al. 2011, *ApJ*, 730, L29
- Morales, F. Y., Padgett, D. L., Bryden, G., Werner, M. W., & Furlan, E. 2012, *ApJ*, 757, 7
- Neugebauer G. et al. 1984, *ApJ*, 278, L1
- Nordström, B., Mayor, M., Andersen, J., et al. 2004, *A&A*, 418, 989
- Onehag A., Korn A., Gustafsson B., Stempels E., Vanden-Berg D.A. 2011, *A&A*, 528, A85
- Oudmaijer, R. D., van der Veen, W. E. C. J., Waters, L. B. F. M., et al. 1992, *A&AS*, 96, 625
- Pasquini, L., Biazzo, K., Bonifacio, P., Randich, S., & Bedin, L. R. 2008, *A&A*, 489, 677
- Patel, R. I., Metchev, S. A., & Heinze, A. 2014, *ApJS*, 212, 10
- Porto de Mello, G. F., & da Silva, L. 1997, *ApJL*, 482, L89
- Ramírez, I., Melendez, J., Cornejo, D., Roederer, I. U., & Fish, J. R. 2011, *ApJ*, 740, 76
- Ramírez, I., Michel, R., Sefako, R., et al. 2012, *ApJ*, 752, 5
- Ramírez, I., Bajkova, A. T., Bobylev, V. V., et al. 2014, *ApJ*, 787, 154
- Ribas, ., Mern, B., Ardila, D. R., & Bouy, H. 2012, *A&A*, 541, A38

- Rieke, G. H., Su, K. Y. L., Stansberry, J. A., et al. 2005, *ApJ*, 620, 1010
- Saffe, C., Gmez, M., Pintado, O., & Gonzlez, E. 2008, *A&A*, 490, 297
- Schneider, J., Dedieu, C., Le Sidaner, P., Savalle, R., & Zolotukhin, I. 2011, *A&A*, 532, A79
- Sierchio, J. M., Rieke, G. H., Su, K. Y. L. & Gspr, A. 2014, *ApJ*, 785, 33
- Stauffer, J. R., Hartmann, L. W., & Barrado y Navascues, D. 1995, *ApJ*, 454, 910
- Su, K. Y. L., Rieke, G. H., Stansberry, J. A., et al. 2006, *ApJ*, 653, 675
- Su, K. Y. L., & Rieke, G. H. 2014, in *IAU Symp. 299, Exploring the Formation and Evolution of Planetary Systems*, ed. M. Booth, B. C. Matthews, & J. R. Graham (Cambridge: Cambridge Univ. Press), 318
- Tisserand, P. 2012, *A&A*, 539, A51
- Trilling D. E. et al., 2008, *ApJ*, 674, 1086
- Urban, L. E., Rieke, G., Su, K., et al. 2012, *ApJ*, 750, 98
- Yana Galarza J., Melndez J., Cohen J.G., 2016a, *A&A*, 589, 65
- Vican, L., & Schneider, A. 2014, *ApJ*, 780, 154
- Wyatt, M. C., Smith, R., Su, K. Y. L., et al. 2007, *ApJ*, 663, 365
- Wyatt, M. C. 2008, *ARA&A*, 46, 339
- Wright E. L. et al., 2010, *AJ*, 140, 1868
- Wu, C. -J., Wu, H., Lam, M.-I., et al. 2013, *ApJS*, 208, 29
- Zuckerman, B., Song, I., Bessell, M. S., & Webb, R. A. 2001, *ApJL*, 562, L87

Zuckerman, B. M., & Song, I. 2004, ApJ, 603, 738

Table 1: *WISE* flux and disc properties.

Star	L_*	Age	J-H	K- [22]	$\frac{F_{12}^d}{F_{12}^{phot}}$	SNR ₁₂	$\frac{F_{22}^d}{F_{22}^{phot}}$	SNR ₂₂	T_d	f_d	R_d	M_d	Ref
	L_\odot	(Myr)	(mag)	(mag)					(K)	($\times 10^{-4}$)	(AU)	(M_\oplus)	
Analog													
HD 39060	9.1	~ 12	0.125	3.512	1.11	165.8	22.43	69.3	150	25.50	10.36	3.00×10^{-2}	1,6
HD 86087	59.3	~ 50	-0.063	1.180	-0.10	74.6	1.55	43.5	175	1.77	19.43	7.33×10^{-3}	1,4
HD 113766	17.3	~ 16	0.131	4.737	11.42	107.8	63.11	87.7	270	199	4.40	4.23×10^{-2}	1,5
HD 181296	22.0	~ 12	-0.052	1.747	-0.02	74.4	3.05	56.1	150	2.11	16.11	6.01×10^{-3}	2,6
HD 218396	7.8	~ 60	0.103	0.387	-0.03	69.8	0.46	30.6	250	0.85	3.45	1.11×10^{-4}	1,8
Siblings candidates													
HD 21216	1.73	~ 3.2	0.198	0.670	-0.01	61.4	0.74	15.8	200	1.94	2.54	1.37×10^{-4}	3,7

Notes. The reference to the stellar luminosity and age are shown in the last column: (1) Chen et al. (2014), (2) Wyatt et al. (2007), (3) MacDonald et al. (2012), (4) Chen et al. (2006), (5) Mamajek et al. (2002), (6) Zuckman et al. (2001), (7) Liu et al. (2015) and (8) Marois et al. (2008). For calculate the luminosity fraction we use $\lambda=12 \mu\text{m}$ (*WISE* W3 band) for HD 113766 and $\lambda=22 \mu\text{m}$ (*WISE* W4 band) for HD 39060, HD 86087, HD 113766, HD 181296 and HD 218396 in the equation 2, where $\nu=c/\lambda$.

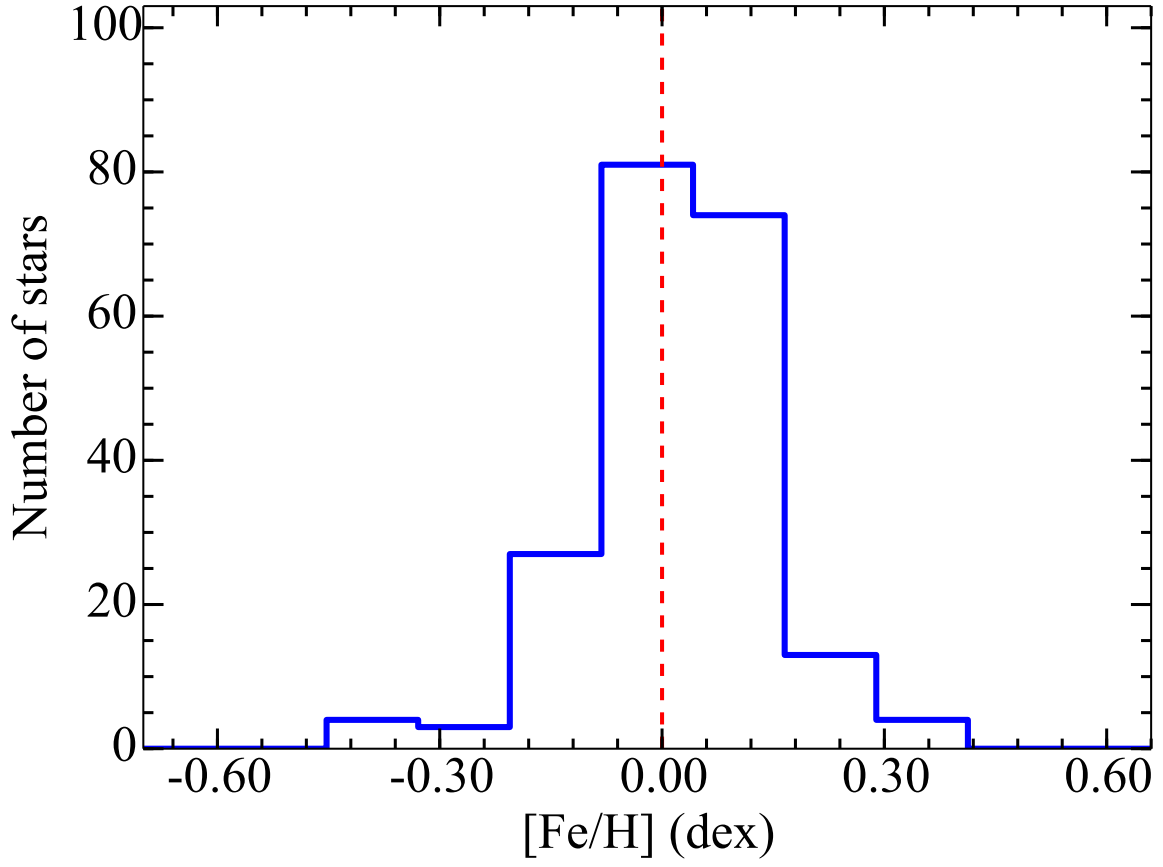


Fig. 1.— Distribution of metallicity for the 206 Sun-like stars analyzed in this work. The canonical solar value is presented by the red dashed line.

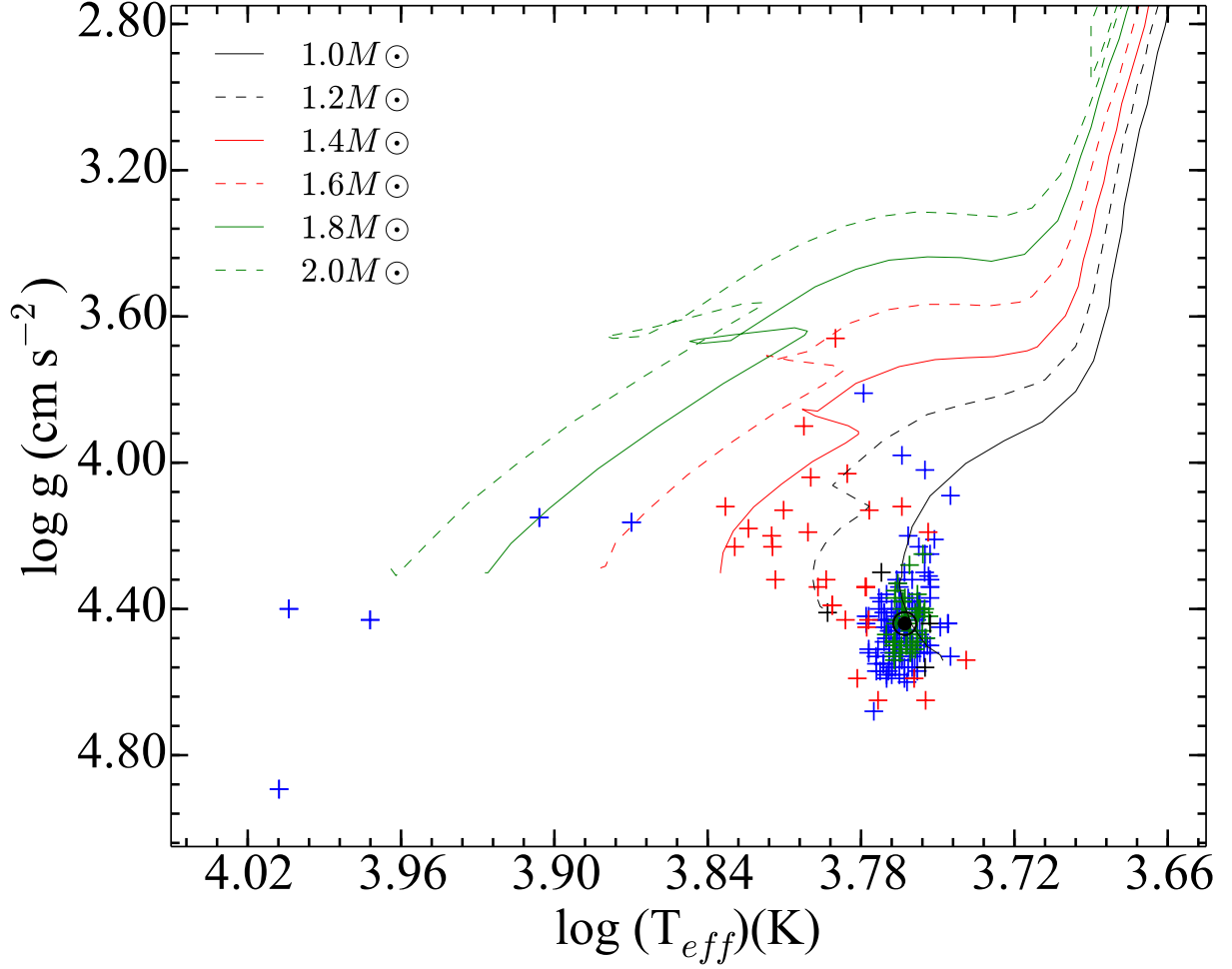


Fig. 2.— Distribution of the 206 Sun-like stars from our sample in a $\log (g)$ vs. $\log (T_{\text{eff}})$ diagram. The solid and dashed lines represent the evolutionary tracks for stars with $[\text{Fe}/\text{H}] = 0$ and masses ranging from 1.0 to $2.0 M_{\odot}$ from Girardi et al. (2000). Stars classified as solar analogs, twins, siblings and sibling candidates are represented by blue, green, black and red symbols, respectively. The position of the Sun is represented by its usual symbol.

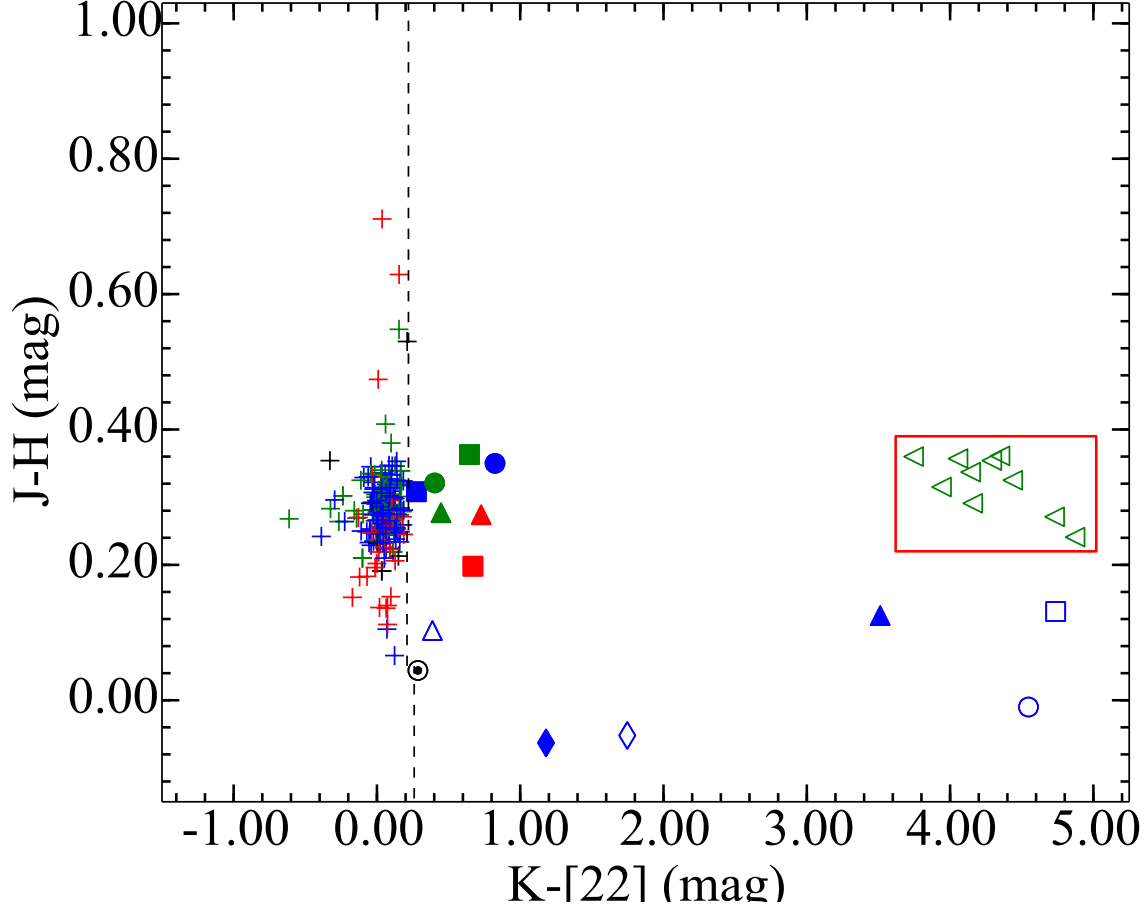


Fig. 3.— Color-color diagram $J - H$ vs. $K - [22]$ for the 216 Sun-like stars that comprise our sample. The colors of the symbols are the same as in Fig. 2. The different symbols represent different stars: red filled square, HD 21216; blue filled triangle, HD 39060; green filled triangle, HD 63487; blue filled diamond, HD 86087; blue circle, HD 109573; blue square, HD 113766; green filled square, HD 145927; green filled circle, HD 150248; red filled triangle HD 168325; blue filled circle, HD 168746; blue diamond, HD 181296 and blue triangle, HD 218396 and blue filled square, HD 224448. The black dashed line shows the criterion to define *WISE* $22\ \mu\text{m}$ excess from Wu et al. (2013), according to which stellar excess candidate should populate the region with $K - [22]$ larger than approximately 0.2. Triangles in the red box represent stars from M67 and they represent upper limits in $K - [22]$.

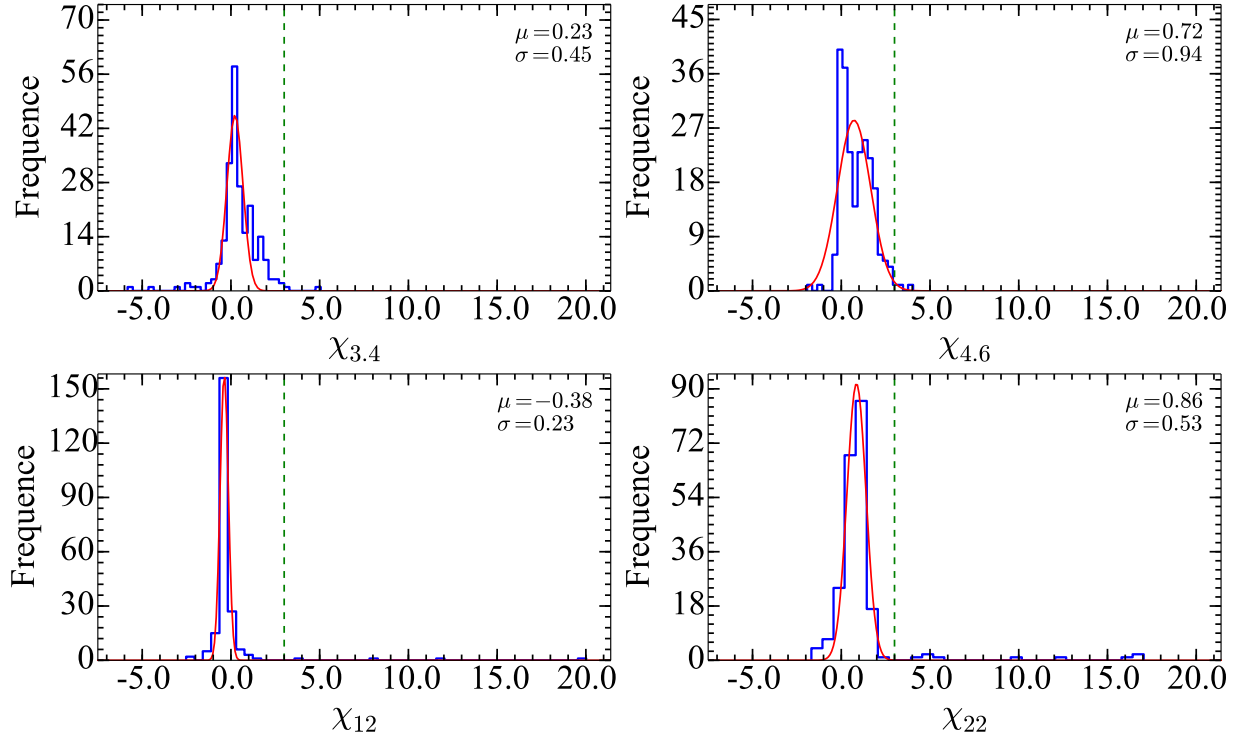


Fig. 4.— Distribution of χ_λ values at 3.4 μm (top left panel), 4.6 μm (top right panel), 12 μm (bottom left panel) and 22 μm (bottom right panel) for stars with $S/N \geq 3$ at the respective wavelength. The green dashed line indicates an excess significance $\chi_\lambda = 3.0$.

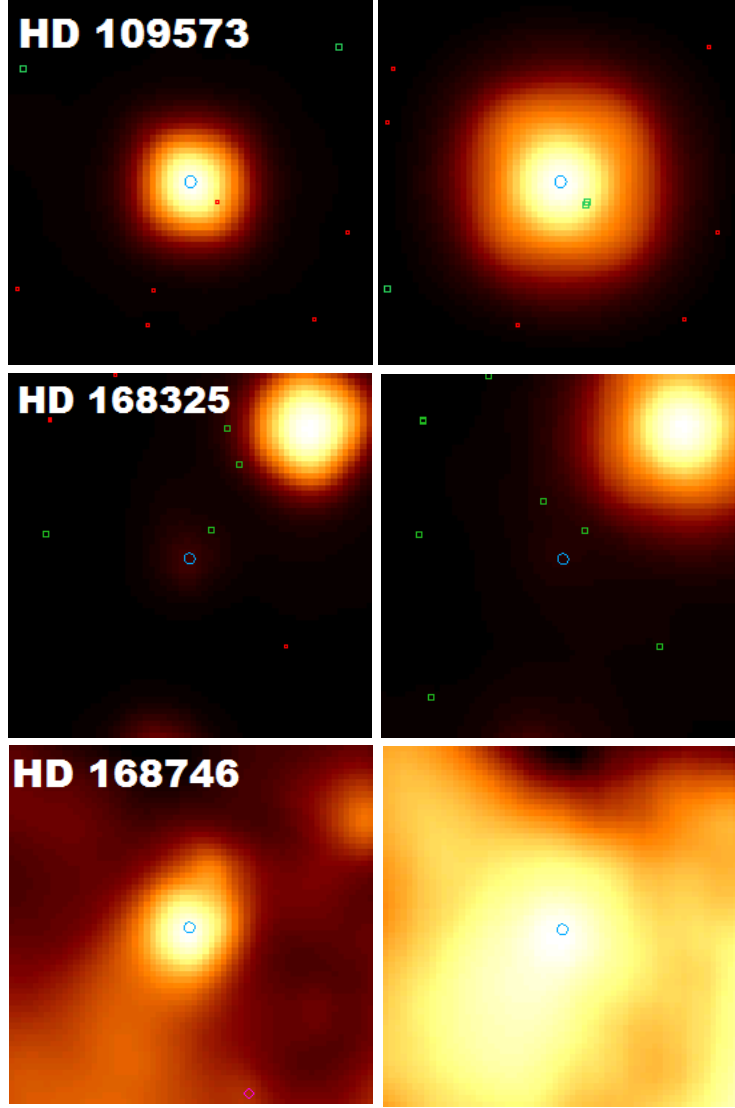


Fig. 5.— *WISE* images (from left to right W3 and W4) in minmax log scales for stars with IR excesses in the 12 and/or 22 μm bands but presenting fundamental problems in the *WISE* images: (top panel) artifact in the W3 and W4 bands for HD 109573; (middle panel) object absent in the W3 and W4 band for HD 168325. (bottom panel) point source without a fundamental problem in the W3 band and contaminated by background emission in the W4 band for HD 168746.

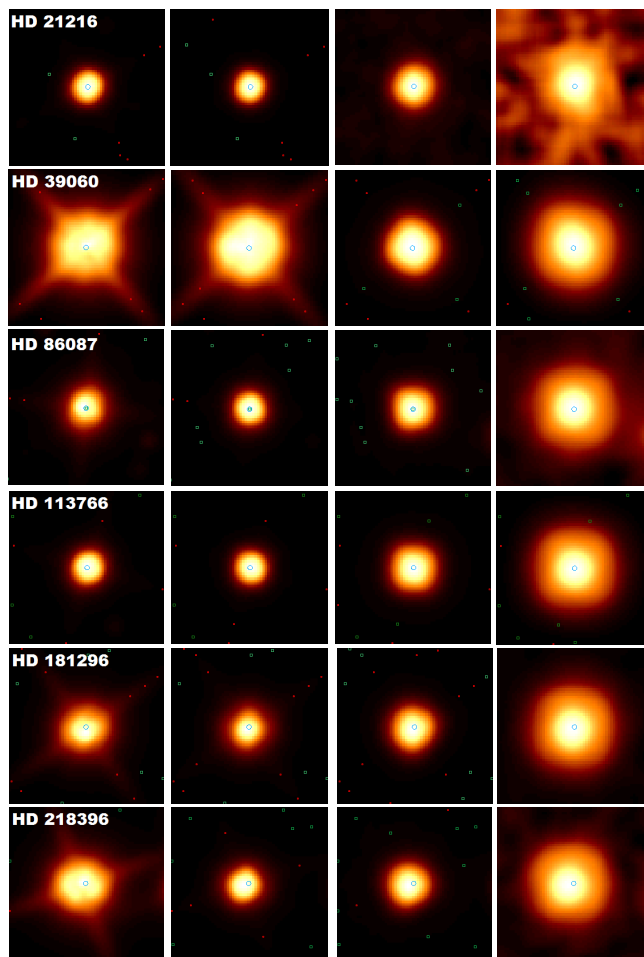


Fig. 6.— *WISE* images (from left to right: W1, W2, W3, and W4) in minmax log scales for 6 stars with infrared excesses in the $22\mu\text{m}$ band that survived the visual image inspection. These stars are examples of clear point sources in all WISE bands. No contamination by artifacts has been found in bands with observed IR excess.

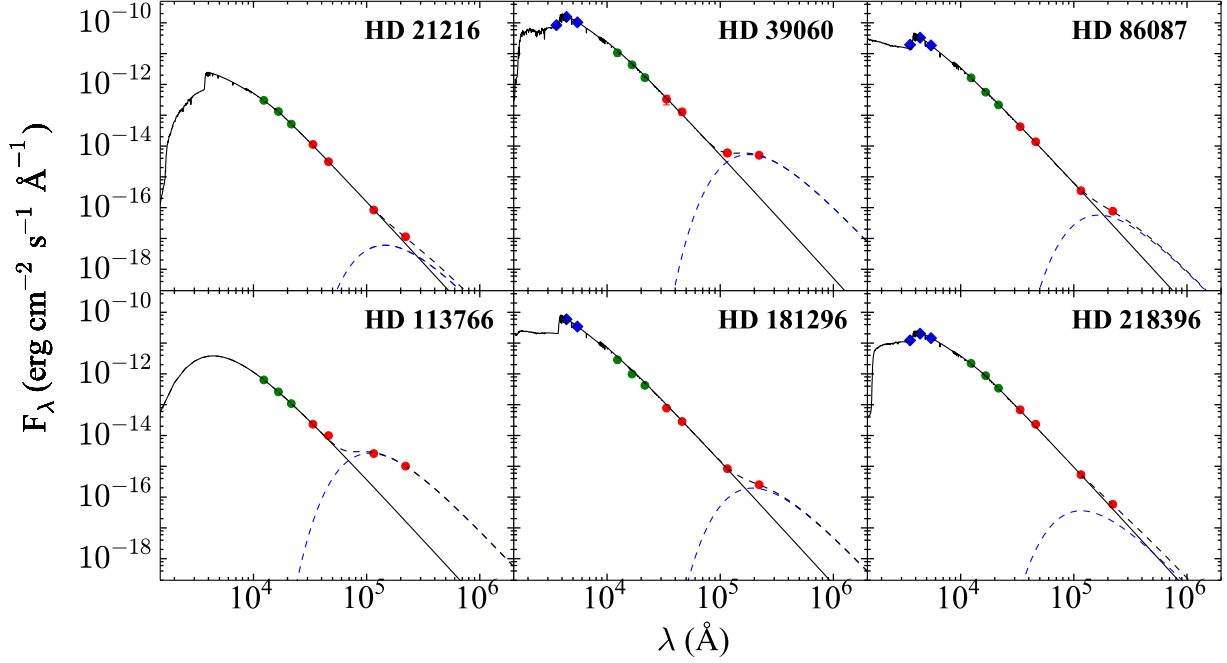


Fig. 7.— SEDs for stars with WISE excesses at the 3σ level of confidence (HD 21216, HD 39060, HD 86087, HD 113766, HD 181296, and HD 218396). The UVB fluxes (Mermilliod 2006) are plotted as blue squares; 2MASS J, H, and K fluxes (Cutri et al. 2013) as green circles; and the WISE bands W1, W2, W3, and W4 (Cutri et al. 2013) as red circles. The black solid line represents the stellar Kurucz model (Castelli et al. 1997). For HD 113766, the stellar Kurucz model does not have enough points to construct a fit, and therefore, we fit the photometry to this star using a black body model (Allard et al. 2012). The blue dashed line shows the best fit using a single black body model for the WISE bands with IR excess, while the black dotted line indicates the sum of the two components.

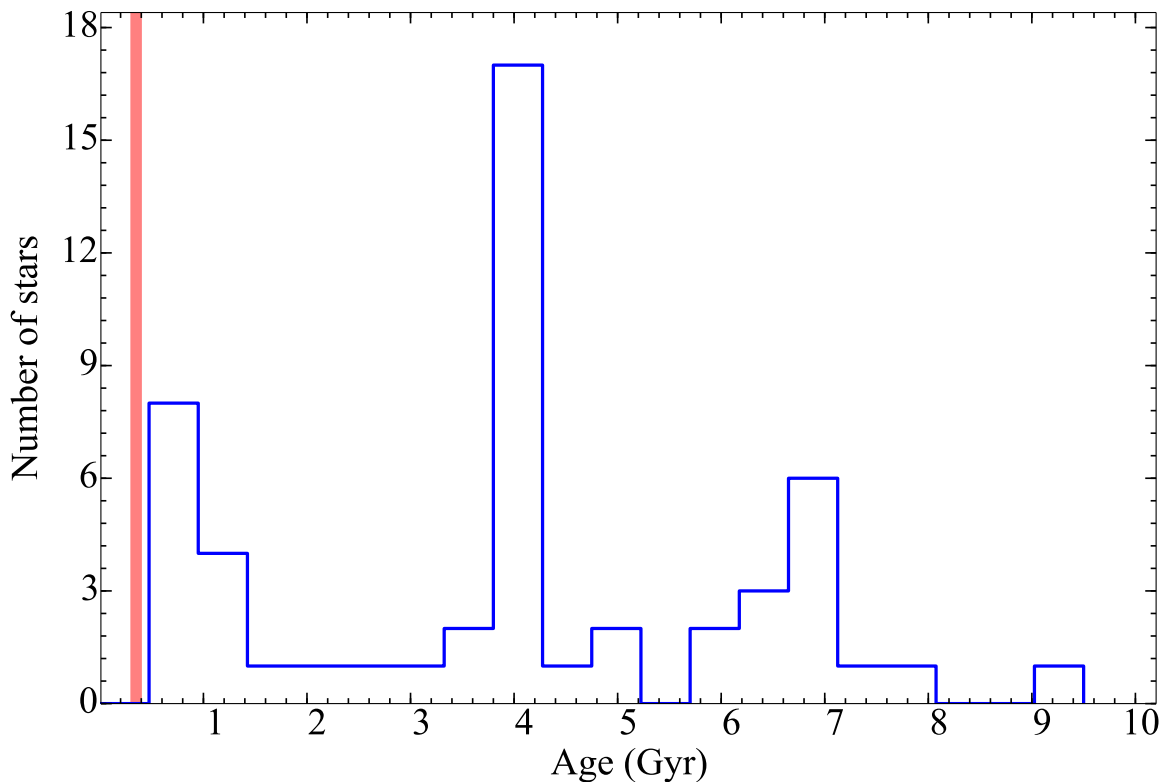


Fig. 8.— Age distribution for the sample of 60 solar twin stars with *WISE* measurements. Ages were taken from Yana Galarza et al. (2016), Ramirez et al. (2014), and Melendez et al. (2006); for stars from Datson et al. (2015) and Pasquini et al. (2008), age were taken from Holmberg et al. (2007) and Önehag et al. (2011), respectively. The shaded region indicates the expected age interval of 300 to 400 Myr for disks disappearance (Habing et al. 1999).

5. Online material

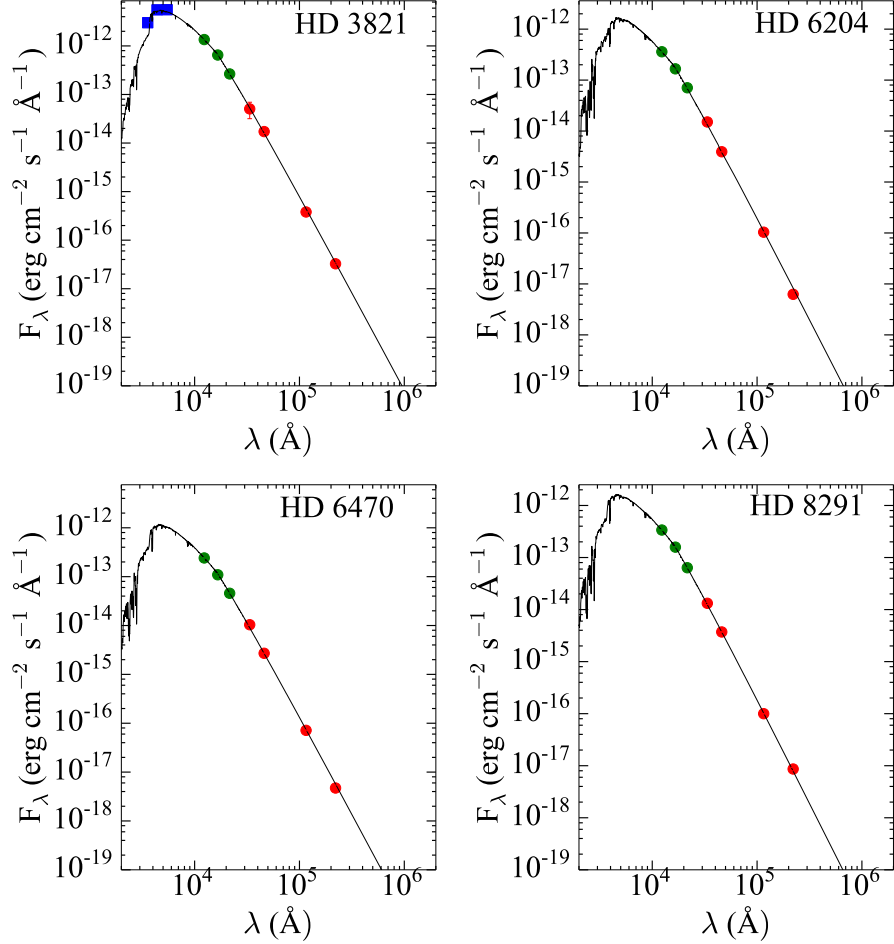


Fig. 9.— SEDs for twin and sibling stars without WISE excesses. The 2MASS J, H, and K fluxes (Cutri et al. 2013) as green circles; and the WISE bands W1, W2, W3, and W4 (Cutri et al. 2013) as red circles. When available, the UBV fluxes (Mermilliod 2006) and SDSS ugriz fluxes (Ahn C. P. et al. 2012) are plotted as blue squares and magenta circle, respectively. Red open triangles presents the WISE upper limits. The black solid line represents the stellar Kurucz model (Castelli et al. 1997).

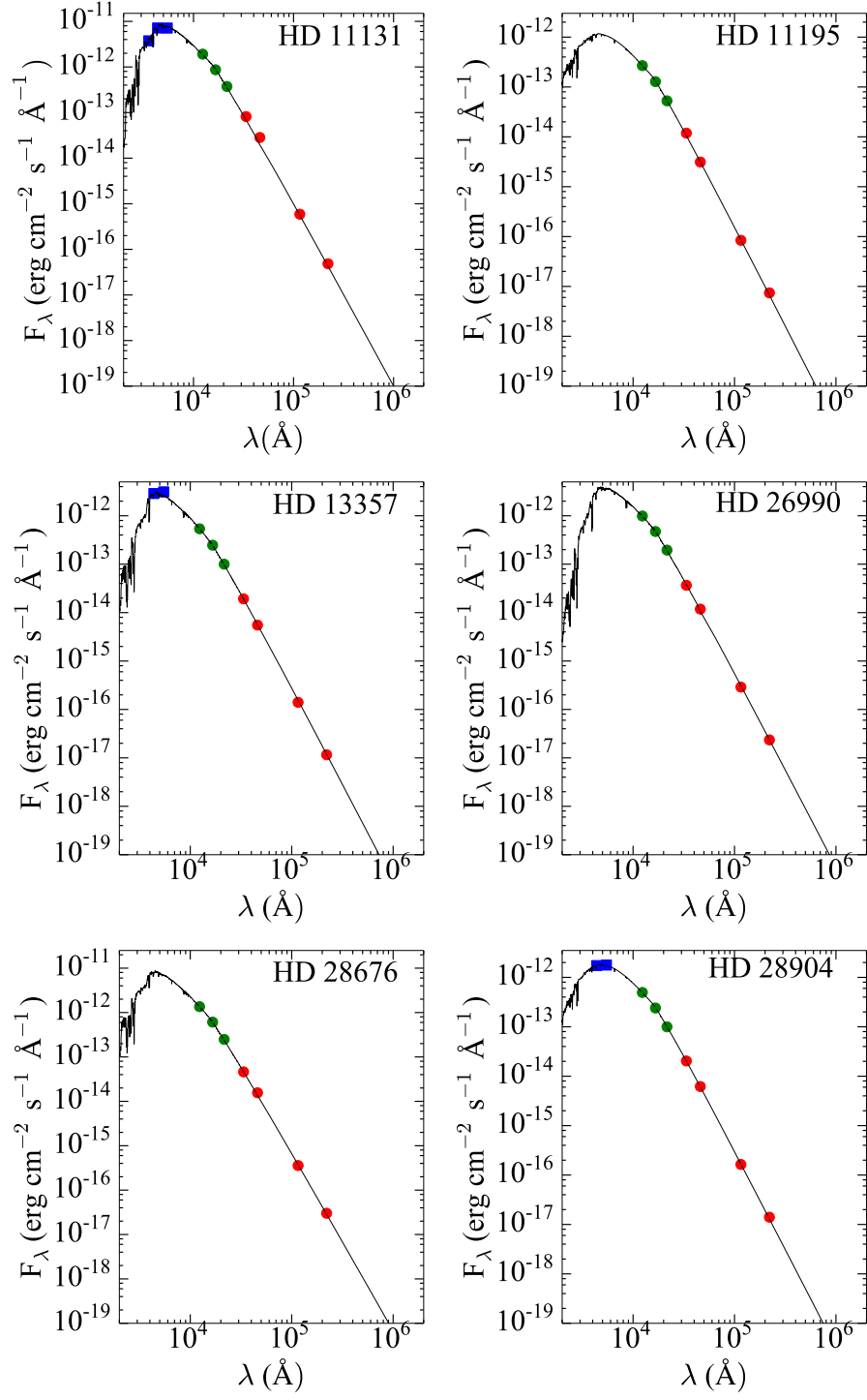


Fig. 10.— Cont. Fig. 9

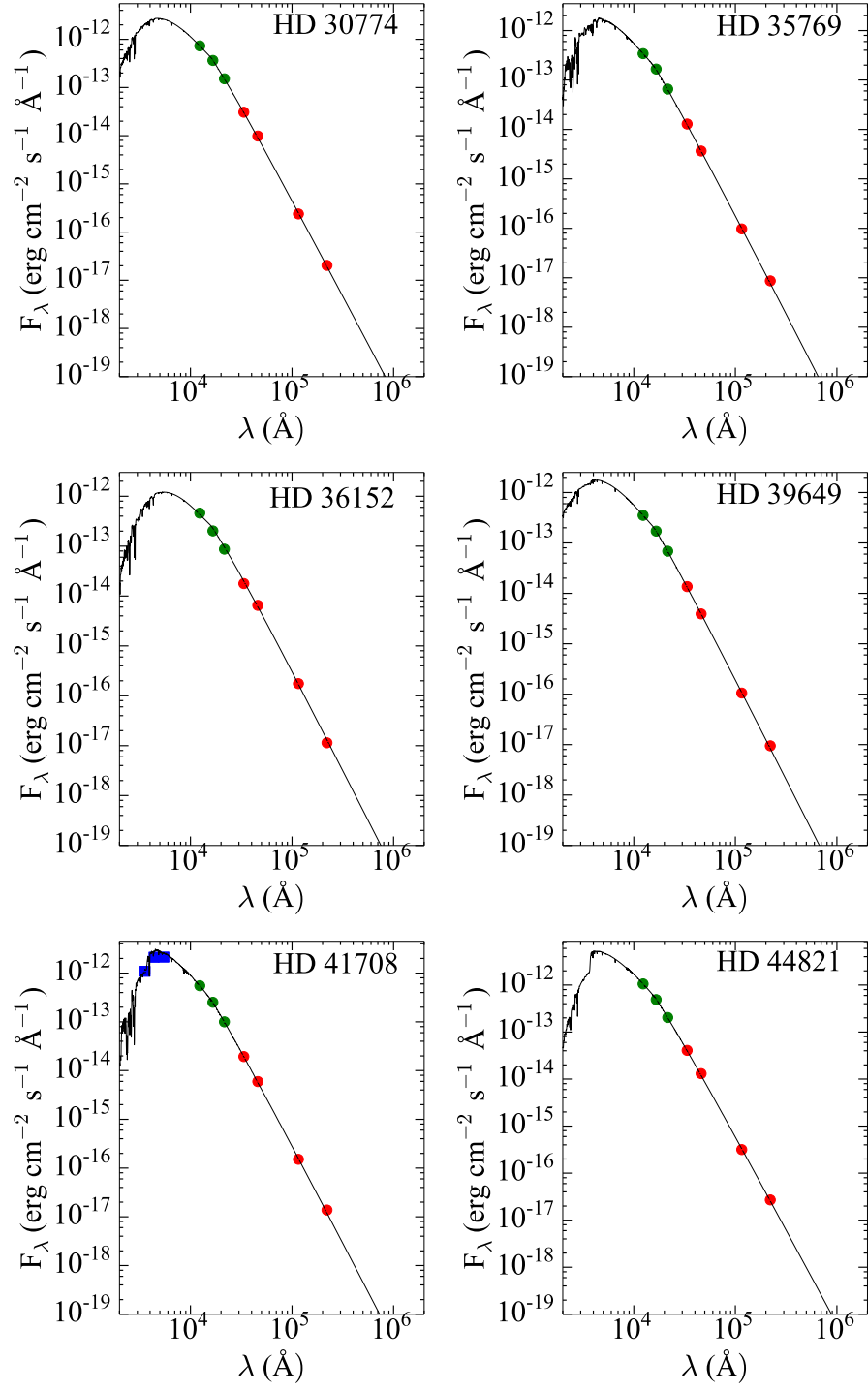


Fig. 11.— Cont. Fig. 9

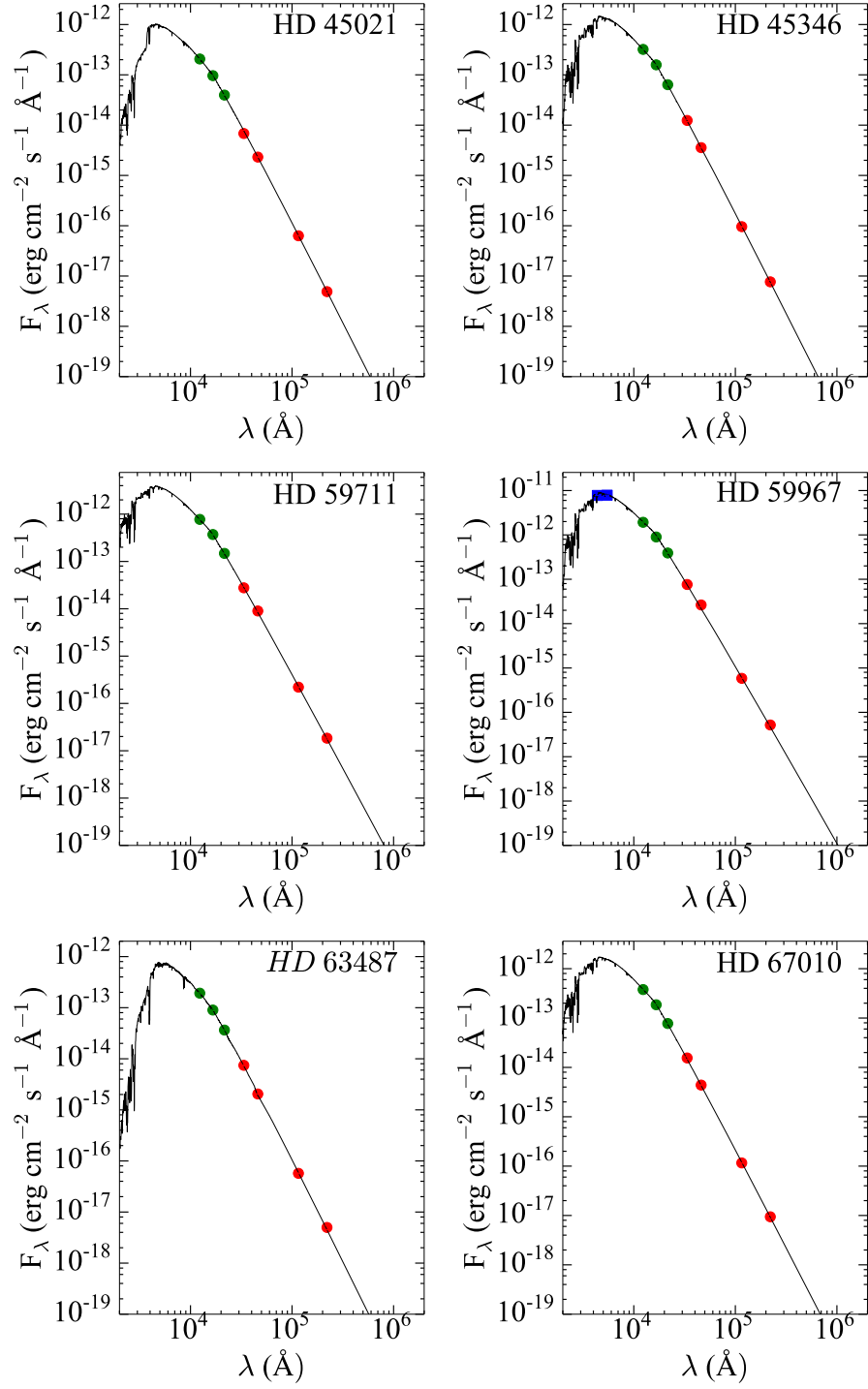


Fig. 12.— Cont. Fig. 9

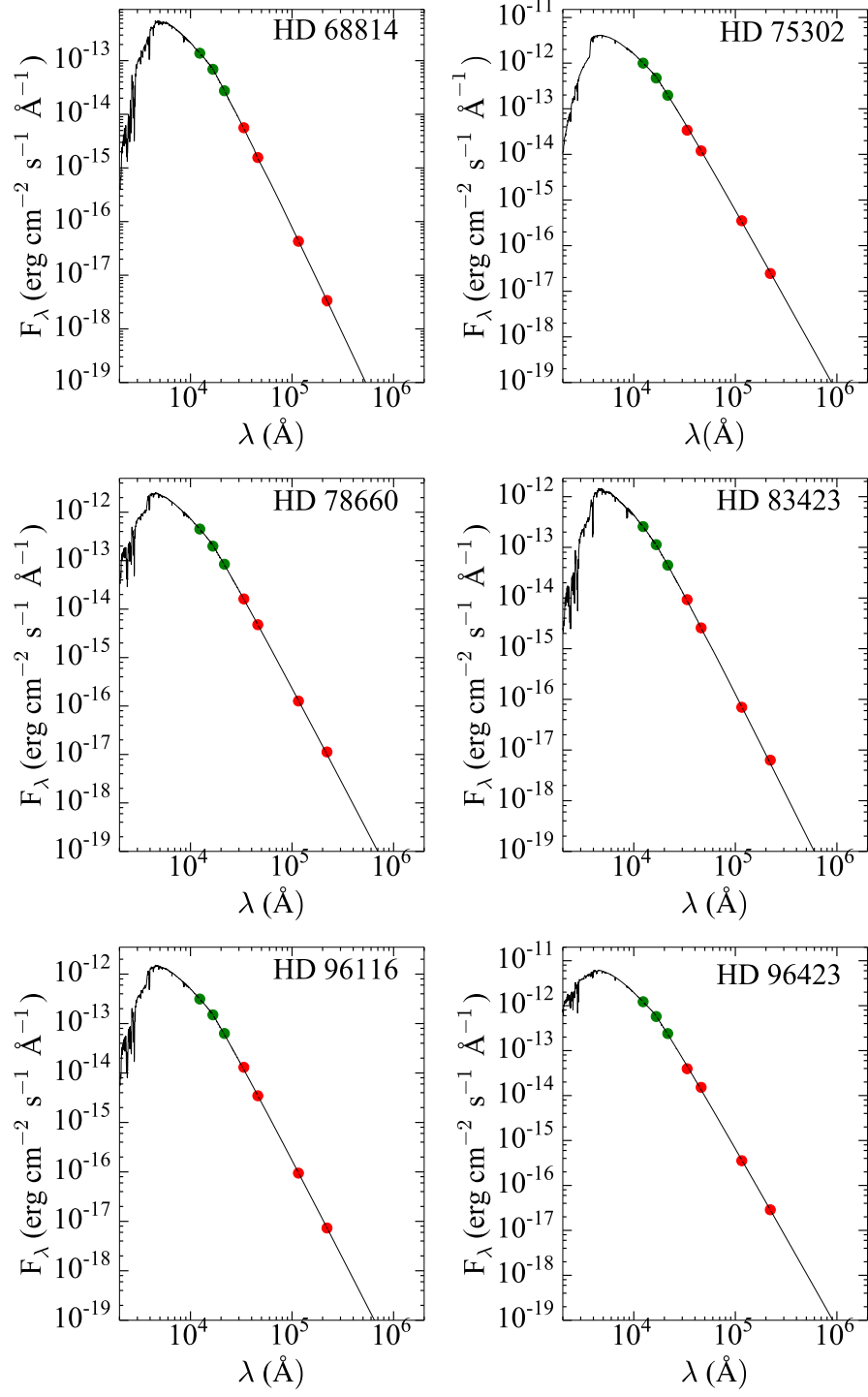


Fig. 13.— Cont. Fig. 9

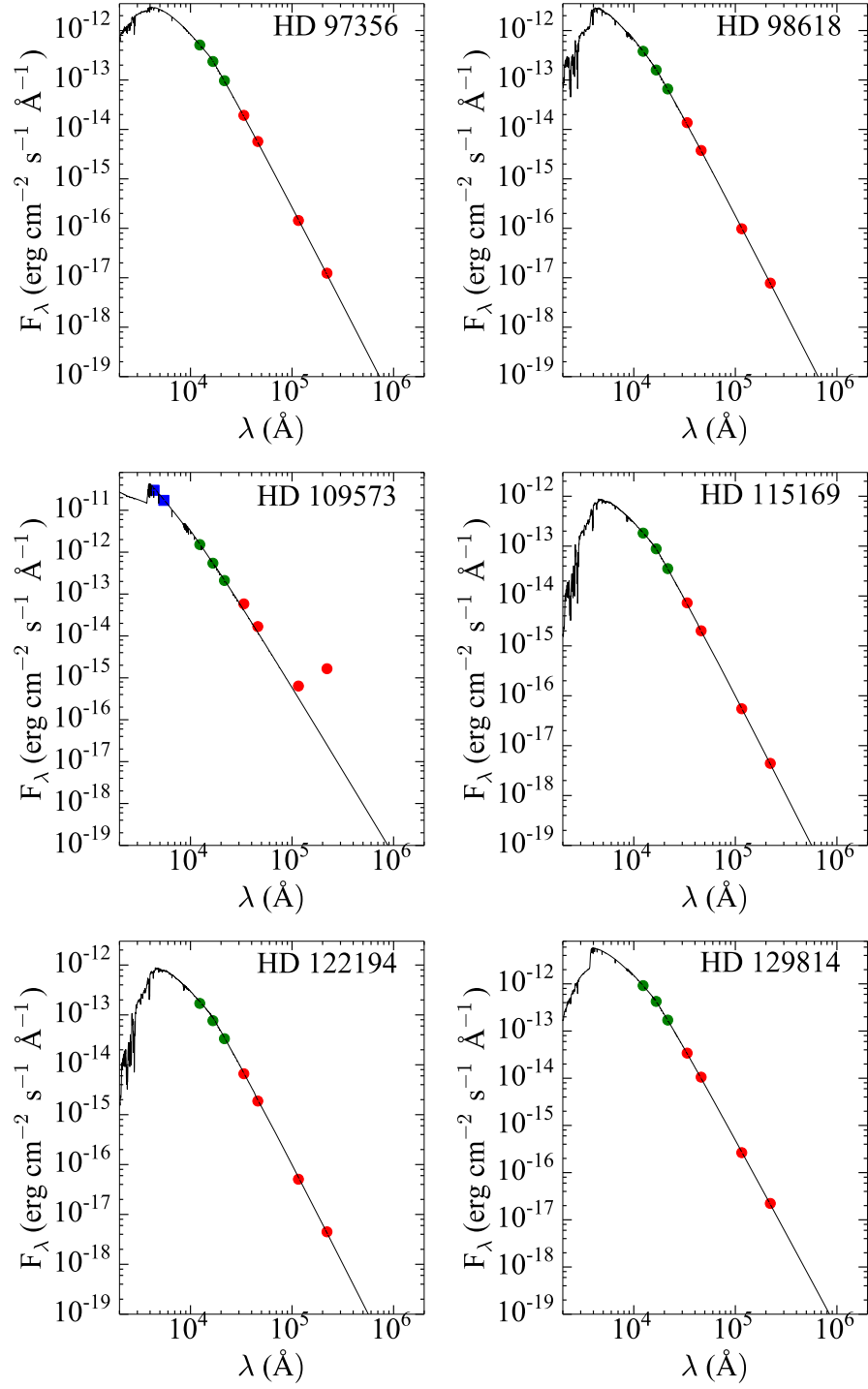


Fig. 14.— Cont. Fig. 9

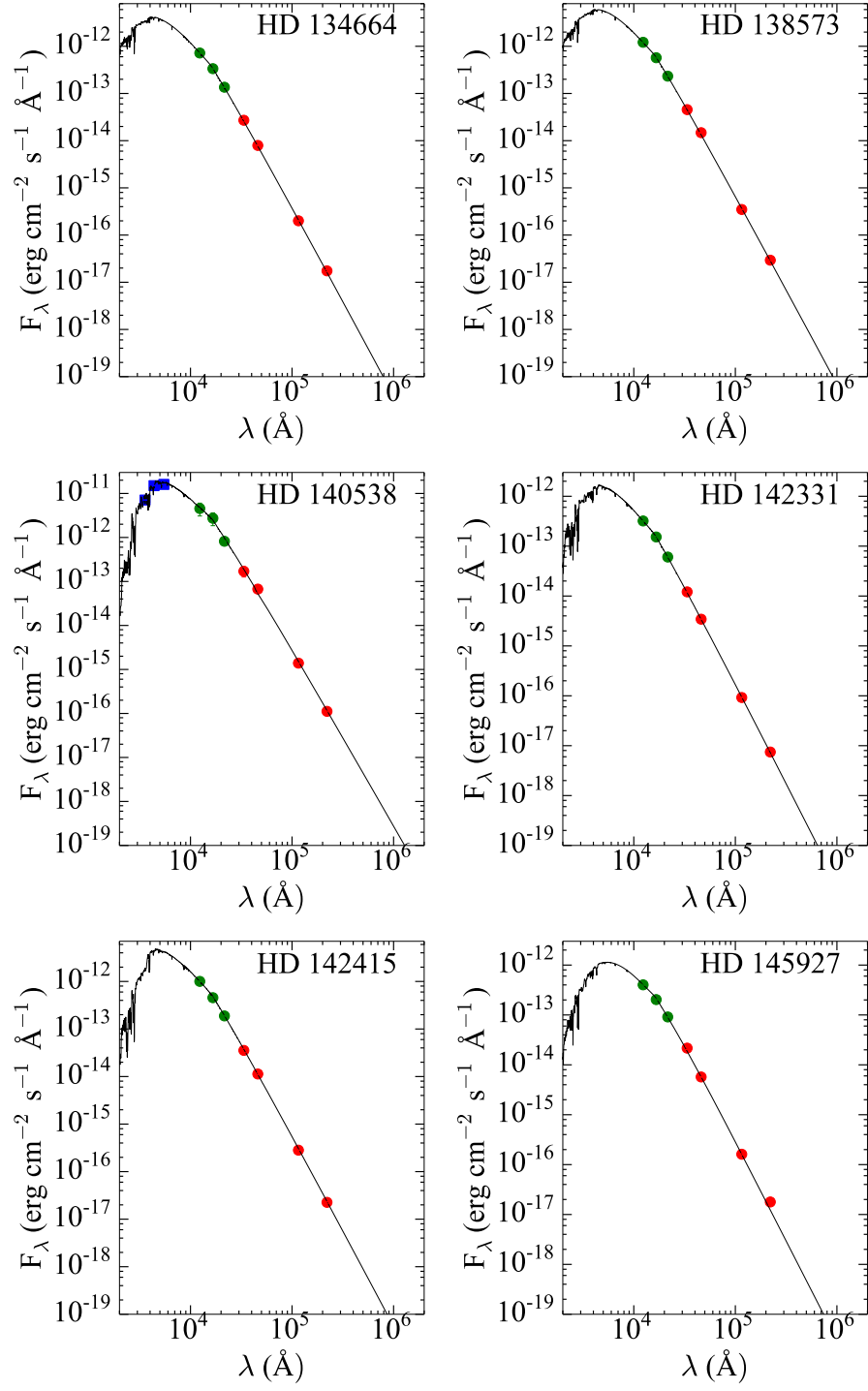


Fig. 15.— Cont. Fig. 9

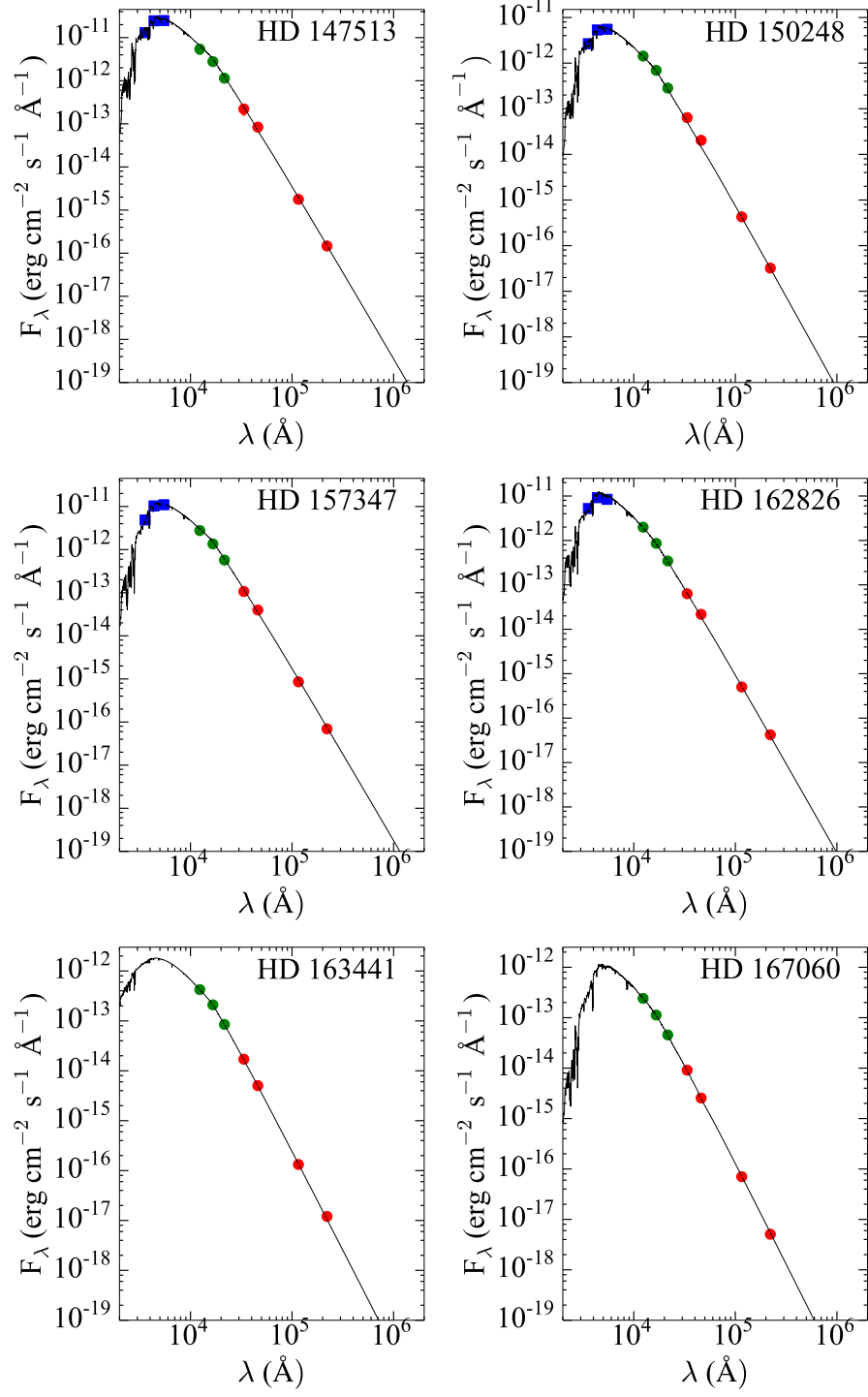


Fig. 16.— Cont. Fig. 9

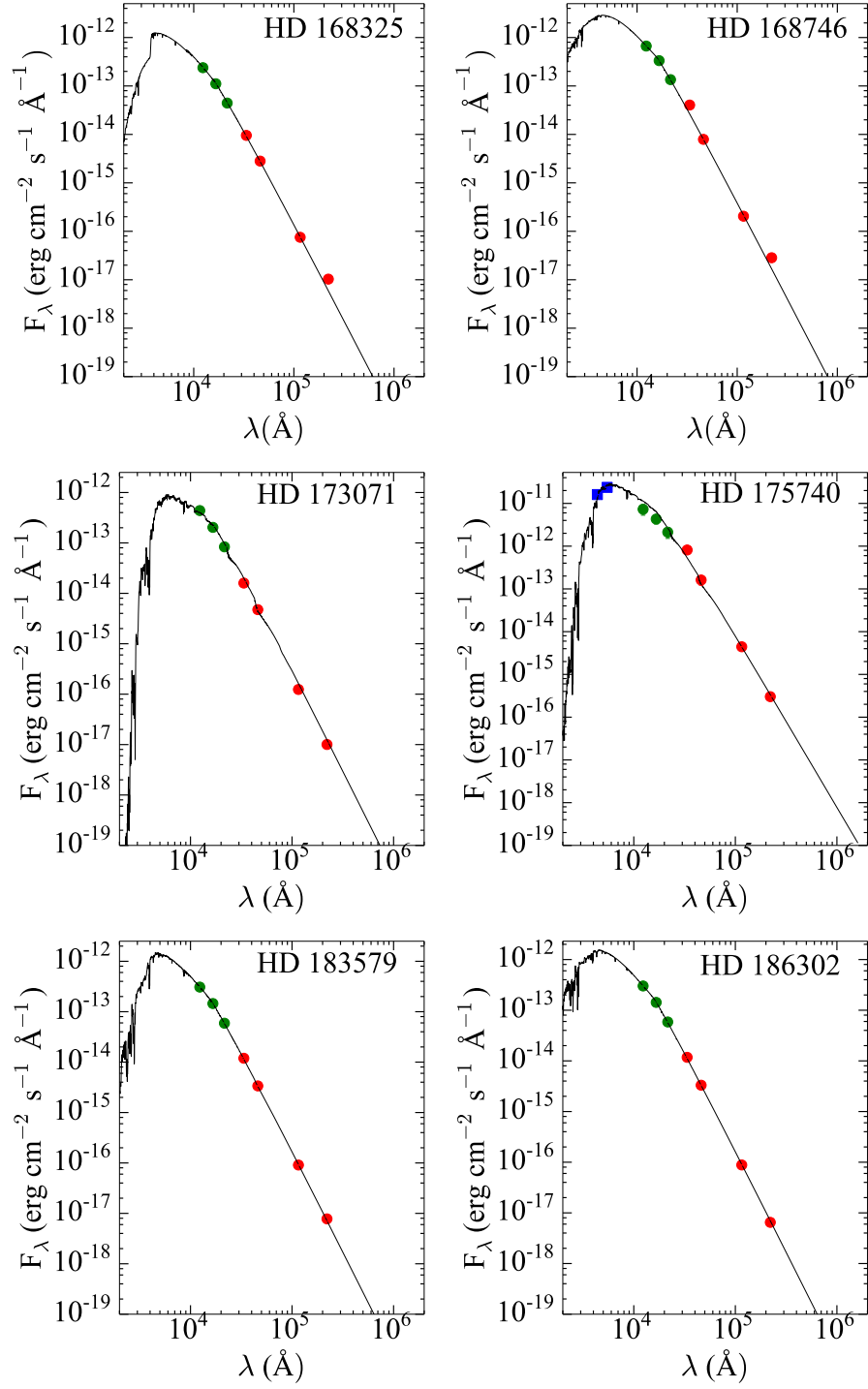


Fig. 17.— Cont. Fig. 9

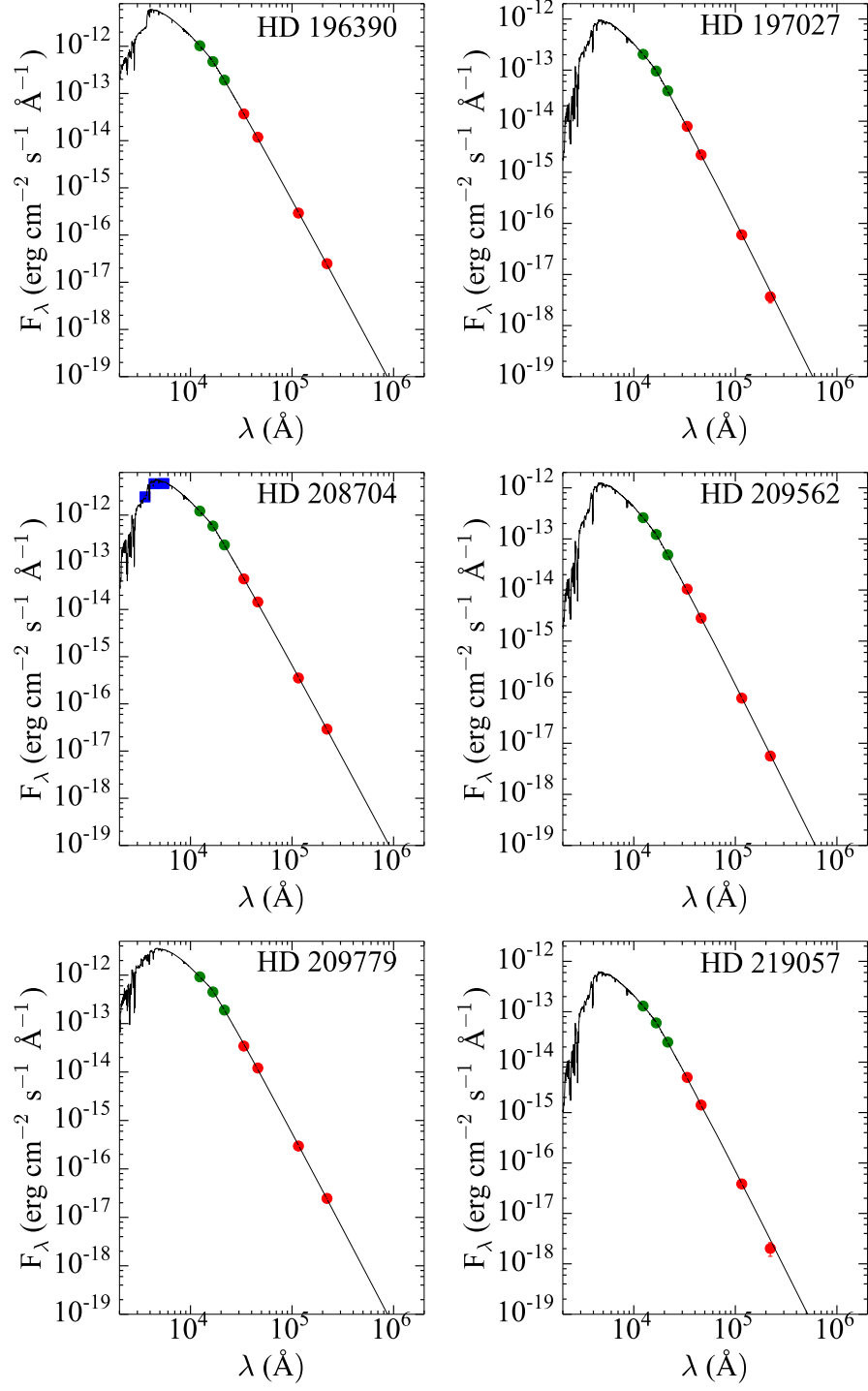


Fig. 18.— Cont. Fig. 9

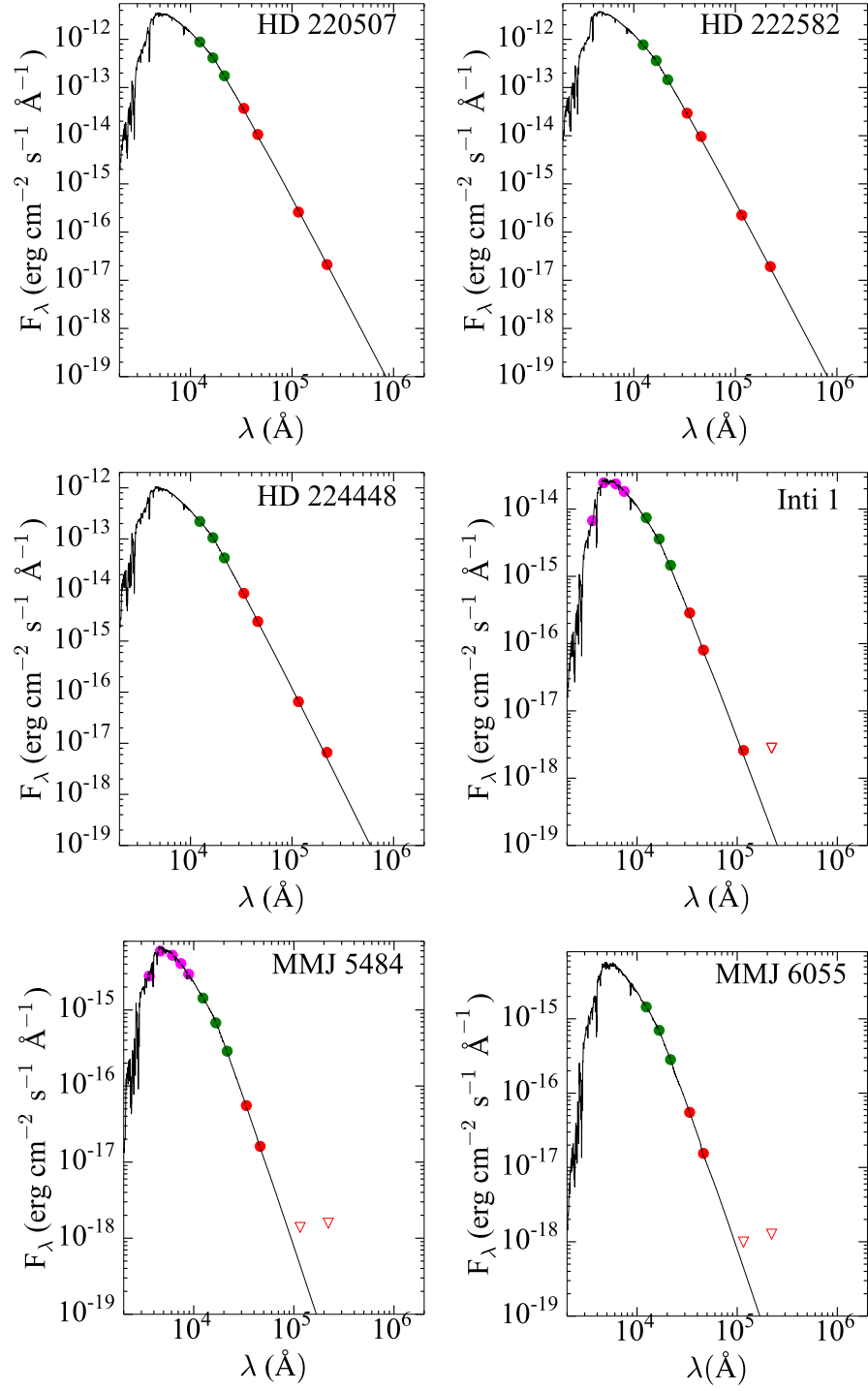


Fig. 19.— Cont. Fig. 9

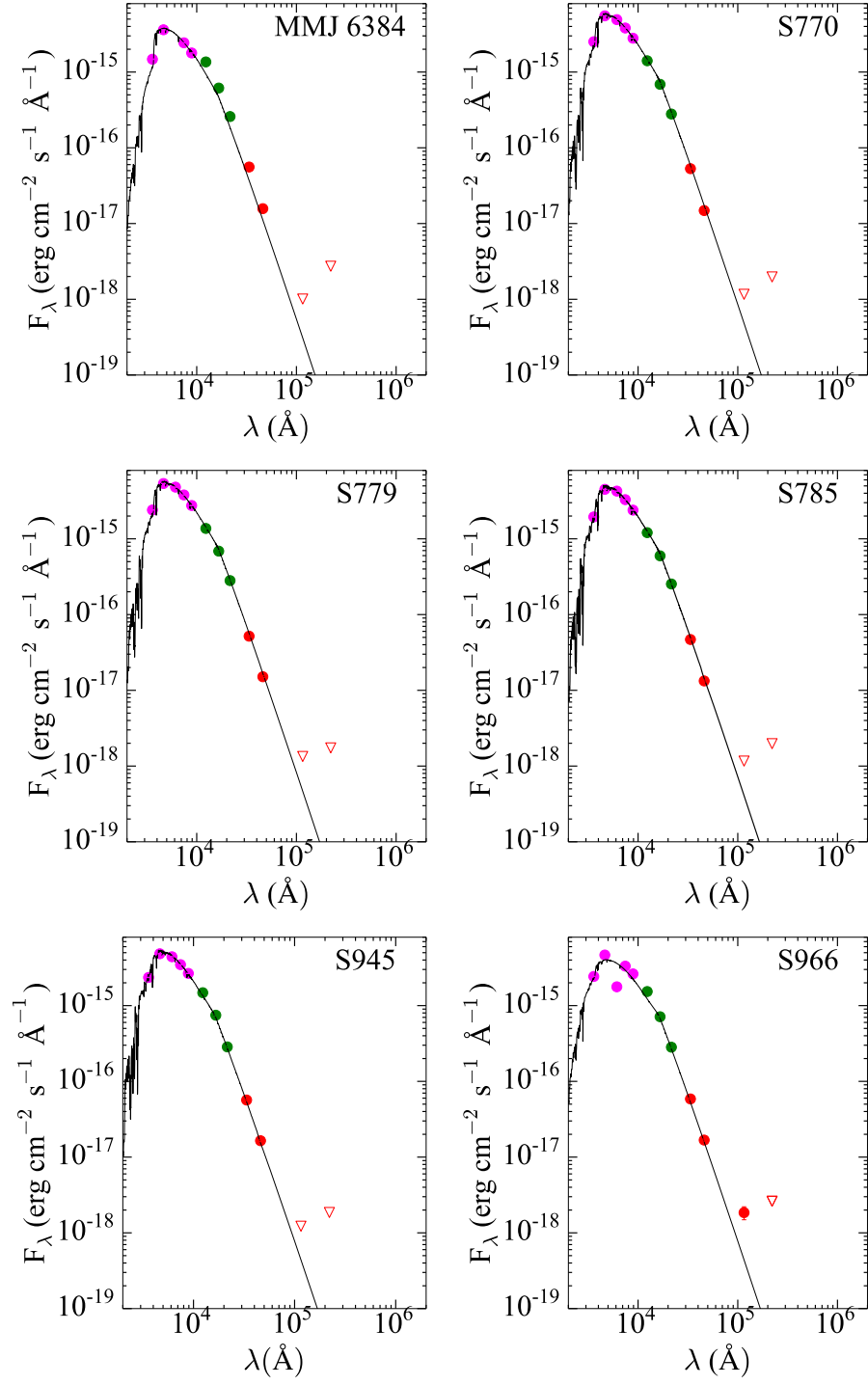


Fig. 20.— Cont. Fig. 9

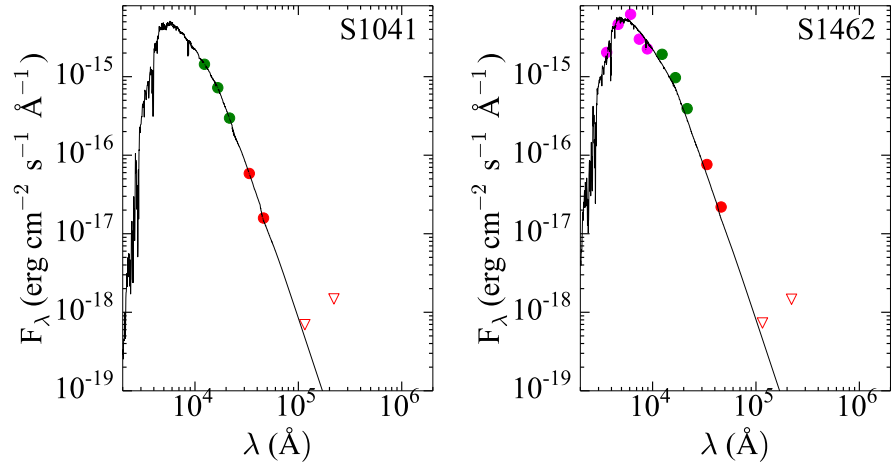


Fig. 21.— Cont. Fig. 9

Table 2: Stellar parameters, including V, 2MASS and WISE magnitudes and excess significance χ_λ for the four WISE bands of the 216 Sun-like stars.

Star	V (mag)	ST	T_{eff} (K)	$\log g$ (cm s^{-2})	[Fe/H] (dex)	Ref	J (mag)	H (mag)	K (mag)	[3.4] (mag)	[4.6] (mag)	[12] (mag)	[22] (mag)	$\chi_{3.4}$	$\chi_{4.6}$	χ_{12}	χ_{22}
Analogues																	
HD4392	7.88	G5V	5656	4.34	0.050	1,1,2,2,2	6.66	6.37	6.25	6.25	6.21	6.26	6.26	-0.281	2.020	-0.553	0.341
HD6470	8.97	G5	5779 \pm 38	4.49 \pm 0.07	-0.190 \pm 0.023	5,1,5,5,5	7.78	7.54	7.43	7.31	7.38	7.41	7.82	3.145	0.145	-0.439	-1.050
HD7678	8.25	G3V	5844	4.52	0.140	1,1,2,2,2	7.12	6.87	6.75	6.69	6.75	6.75	6.68	0.553	0.347	-0.333	0.571
HD8076	7.65	G2V	5893	4.43	0.050	1,1,2,2,2	6.56	6.26	6.19	6.19	6.18	6.20	6.16	-1.812	2.156	-0.186	-0.113
HD9986	6.77	G5V	5828	4.49	0.110	1,1,2,2,2	5.62	5.33	5.22	5.21	5.03	5.27	5.25	0.106	2.426	-0.709	0.459
HD10180	7.33	G1V	5891	4.36	0.070	1,1,2,2,2	6.25	5.93	5.87	5.81	5.80	5.86	5.83	0.142	1.047	-0.379	0.747
HD11131	6.72	G0	5804	4.53	-0.090	1,1,2,2,2	5.54	5.29	5.15	4.99	4.79	5.11	5.07	0.744	4.339	1.399	2.197
HD12264	7.99	G5V	5819	4.47	0.050	1,1,2,2,2	6.82	6.54	6.45	6.38	6.42	6.45	6.39	0.301	1.415	-0.638	1.102
HD13724	7.89	G3/G5V	5809	4.54	0.250	1,1,2,2,2	6.73	6.48	6.38	6.27	6.35	6.38	6.30	0.613	2.507	-0.567	1.399
HD15632	8.03	G0	5762	4.51	0.030	1,1,2,2,2	6.81	6.55	6.47	6.47	6.47	6.49	6.39	0.174	1.023	-0.483	1.399
HD18330	7.90	F5	5989	4.52	-0.030	1,1,2,2,2	6.80	6.55	6.46	6.44	6.46	6.48	6.45	0.150	1.225	-0.492	0.645
HD19617	8.69	G5	5727	4.38	0.150	1,1,2,2,2	7.45	7.20	7.11	7.03	7.11	7.11	7.12	1.035	-0.030	-0.104	-0.285
HD20201	7.27	G0V	5994	4.44	0.100	1,1,2,2,2	6.21	5.98	5.88	5.83	5.79	5.90	5.86	0.197	1.432	-0.395	0.847
HD20527	8.70	G5	5615	4.45	0.110	1,1,2,2,2	7.44	7.12	7.08	6.92	7.00	7.02	6.92	1.629	0.378	-0.242	1.301
HD24552	7.97	G0	5825	4.44	-0.060	1,1,2,2,2	6.86	6.63	6.49	6.49	6.49	6.52	6.47	-0.269	0.682	-0.512	0.797
HD25710	8.11	G0	5994	4.42	-0.090	1,1,2,2,2	7.00	6.78	6.65	6.61	6.64	6.65	6.59	-5.823	1.102	-0.362	1.007
HD25926	7.70	G2V	5915	4.38	-0.010	1,1,2,2,2	6.56	6.30	6.19	6.14	6.11	6.17	6.12	-0.021	1.981	-0.443	0.875
HD26767	8.05	G0	5792	4.30	0.080	1,1,2,2,2	6.86	6.61	6.53	6.50	6.55	6.53	6.37	-0.083	0.742	-0.713	1.100
HD27685	7.86	G4V	5705	4.42	0.070	1,1,2,2,2	6.58	6.33	6.20	6.18	6.18	6.22	6.14	-0.718	0.668	-1.388	0.731
HD28068	8.04	G1V	5761	4.32	0.070	1,1,2,2,2	6.84	6.56	6.44	6.36	6.39	6.42	6.41	-0.010	0.516	-0.586	0.635
HD28099	8.10	G8V	5718	4.38	0.060	1,1,2,2,2	6.89	6.64	6.55	6.54	6.55	6.58	6.66	-0.414	1.408	-0.446	0.021
HD29150	7.58	G5	5755	4.48	-0.020	1,1,2,2,2	6.38	6.08	5.99	6.01	5.92	6.01	5.95	-0.677	1.293	-0.318	0.878
HD29161	7.88	G0	5890	4.59	-0.030	1,1,2,2,2	6.77	6.49	6.41	6.34	6.38	6.41	6.39	0.238	0.740	-0.396	0.610
HD29461	7.96	G5	5766	4.38	0.160	1,1,2,2,2	6.81	6.52	6.44	6.37	6.42	6.44	6.44	0.464	1.595	-0.400	0.443
HD30246	8.30	G5	5723	4.52	0.080	1,1,2,2,2	7.10	6.84	6.74	6.75	6.75	6.76	6.69	0.190	1.764	0.326	1.213

Star	V (mag)	ST	T _{eff} (K)	log g (cm s ⁻²)	[Fe/H] (dex)	Ref	J (mag)	H (mag)	K (mag)	[3.4] (mag)	[4.6] (mag)	[12] (mag)	[22] (mag)	χ _{3.4}	χ _{4.6}	χ ₁₂	χ ₂₂
HD30306	7.76	G6V	5557	4.53	0.170	1,1,2,2,2	6.49	6.15	6.06	5.98	6.02	6.06	6.03	0.288	0.998	-0.387	0.024
HD31222	8.66	G5	5659	4.50	0.120	3,1,4,2,2,2	7.41	7.17	7.08	7.04	7.12	7.10	7.10	1.064	0.151	-0.253	0.494
HD31622	8.49	G5	5823	4.52	-0.170	1,1,2,2,2	7.35	7.10	6.98	6.93	6.96	6.98	6.91	0.632	0.384	-0.213	1.270
HD32963	7.60	G5IV	5710	4.42	0.070	1,1,2,2,2	6.42	6.10	6.02	5.96	6.00	6.06	6.05	0.283	1.852	-0.058	0.939
HD33866	7.82	G2V	5836	4.45	-0.030	1,1,2,2,2	6.57	6.24	6.13	6.05	6.08	6.12	6.11	0.235	2.016	-0.349	0.432
HD33873	8.65	G6V	5658	4.37	0.190	1,1,2,2,2	7.42	7.14	7.02	6.98	7.04	7.02	7.05	0.648	-0.277	-0.063	0.804
HD34239	7.10	G0V	5932	4.40	0.040	4,1,4,2,2,2	6.01	5.75	5.63	5.62	5.51	5.65	5.58	-0.849	1.290	-0.389	0.994
HD34386	8.54	G5III	5689	4.25	0.070	1,1,2,2,2	7.37	7.14	7.04	6.99	7.04	7.04	6.88	0.802	0.377	-0.255	0.967
HD34599	8.28	G3V	5834	4.40	0.080	1,1,2,2,2	7.13	6.83	6.78	6.71	6.76	6.76	6.73	0.334	-0.089	-0.122	0.719
HD36553	5.46	G3IV	6017	3.81	0.320	1,1,2,2,2	4.39	4.29	4.11	4.02	3.52	4.06	4.04	0.088	2.049	0.787	1.679
HD39060	3.86	A3V	8052	4.15	0.110	9,1,10,10,17	3.67	3.54	3.53	3.48	3.18	2.56	0.01	-0.248	0.715	1.159	16.260
HD39833	7.65	G0III	5821	4.38	0.160	1,1,2,2,2	6.49	6.23	6.15	6.13	6.12	6.16	6.08	-0.199	1.646	-0.497	50.018
HD46090	7.14	G0	5778	4.46	0.010	1,1,2,2,2	5.86	5.52	5.40	5.33	5.16	5.42	5.44	-0.253	1.925	-0.419	0.098
HD55693	7.17	G1V	5855	4.40	0.240	1,1,2,2,2	6.04	5.78	5.70	5.70	5.60	5.70	5.63	-0.747	1.360	-0.365	1.224
HD58895	6.58	G5IV	5690	4.02	0.240	1,1,2,2,2	5.40	5.13	5.02	5.00	4.72	5.01	4.90	0.031	1.651	-1.414	1.264
HD5967	6.66	G3V	5860	4.58	-0.030	1,1,2,2,2	5.53	5.25	5.10	5.05	4.84	5.10	4.94	0.124	1.952	-0.418	2.033
HD63433	6.90	G5IV	5693 ± 58	4.52 ± 0.07	0.007 ± 0.025	5,1,5,5,5	5.62	5.36	5.26	5.20	5.05	5.29	5.17	0.126	1.378	-0.662	1.612
HD64474	7.83	G6V	5656	4.25	-0.020	4,1,4,2,2,2	6.58	6.32	6.17	6.19	6.20	6.21	6.13	-0.289	1.245	-0.604	0.818
HD64942	8.37	G5	5839	4.45	0.040	1,1,2,2,2	7.25	6.97	6.87	6.82	6.84	6.87	6.76	0.433	0.436	-0.369	1.461
HD67578	8.60	G2V	5835 ± 30	4.48 ± 0.06	-0.200 ± 0.030	5,1,5,5,5	7.42	7.15	7.08	7.03	7.06	7.06	7.05	1.924	0.111	-0.174	0.305
HD72905	5.6	G1.5Vb	5864 ± 47	4.46 ± 0.09	-0.052 ± 0.026	5,1,5,5,5	4.35	4.28	4.17	4.14	3.70	4.17	4.05	-0.227	1.916	-1.008	1.098
HD75288	8.51	G3/G5V	5775 ± 30	4.37 ± 0.06	0.120 ± 0.030	5,1,5,5,5	7.28	6.94	6.93	6.87	6.94	6.93	6.82	1.249	-0.114	-0.279	1.583
HD76332	8.58	G2V	5827	4.34	-0.060	1,1,2,2,2	7.29	6.97	6.84	6.80	6.81	6.80	6.75	0.369	0.720	-0.025	-0.248
HD76780	7.63	G5	5745	4.40	0.110	5,1,5,5,5	6.41	6.17	6.07	5.97	5.96	6.05	5.93	0.382	2.868	-0.344	0.984
HD77006	7.93	G5	5934 ± 49	4.51 ± 0.06	-0.020 ± 0.019	5,1,5,5,5	6.75	6.41	6.36	6.32	6.30	6.32	6.25	-0.346	1.454	-0.406	0.756

Star	V (mag)	ST	T _{eff} (K)	log g (cm s ⁻²)	[Fe/H] (dex)	Ref	J (mag)	H (mag)	K (mag)	[3.4] (mag)	[4.6] (mag)	[12] (mag)	[22] (mag)	χ _{3.4}	χ _{4.6}	χ ₁₂	χ ₂₂
HD77461	8.83	G3V	5835	4.49	-0.020	3,19,2,2,2	7.49	7.19	7.12	7.07	7.13	7.11	7.00	1.798	0.084	-0.254	0.913
HD78317	8.15	F8	5848	4.43	0.050	1,1,2,2,2	7.06	6.73	6.71	6.60	6.67	6.70	6.65	2.426	0.859	-0.713	1.045
HD78538	8.15	G5	5800	4.59	-0.020	1,1,2,2,2	6.99	6.74	6.63	6.58	6.61	6.61	6.70	0.203	1.135	-0.252	-0.312
HD80533	8.93	G0	5709 ± 65	4.49 ± 0.12	-0.070 ± 0.039	5,1,5,5,5	7.70	7.39	7.34	7.28	7.31	7.31	7.36	1.588	-0.063	-0.182	0.016
HD81659	7.91	G6/G8V	5658	4.52	0.230	1,1,2,2,2	6.69	6.41	6.31	6.24	6.32	6.32	6.29	0.521	2.231	-0.490	0.566
HD81700	8.51	G2V	5890 ± 30	4.48 ± 0.06	0.140 ± 0.030	5,1,5,5,5	7.35	7.10	7.01	6.80	6.88	6.88	6.89	1.337	0.929	0.051	0.694
HD86087	5.71	A0V	10500	4.00	0.080	1,1,11,11,17	5.70	5.77	5.74	5.71	5.61	5.66	4.56	-1.302	-1.924	-2.463	9.890
HD86226	7.93	G2V	5934	4.37	0.010	1,1,2,2,2	6.84	6.58	6.46	6.44	6.45	6.45	6.40	0.002	1.307	-0.465	0.644
HD89454	8.03	G5	5690	4.48	0.100	1,1,2,2,2	6.81	6.54	6.46	6.42	6.44	6.45	6.46	0.231	1.921	-0.391	0.233
HD90722	7.88	G5/G6IV	5720 ± 25	4.23 ± 0.05	0.360 ± 0.030	5,1,5,5,5	6.62	6.34	6.26	6.22	6.25	6.26	6.23	0.216	1.729	-0.446	0.227
HD90936	8.37	G3V	5918	4.43	0.070	1,1,2,2,2	7.24	6.99	6.91	6.87	6.91	6.93	6.96	1.161	0.411	-0.327	-0.030
HD91489	8.44	G2/G3V	5884	4.48	-0.010	1,1,2,2,2	7.30	6.97	6.93	6.86	6.91	6.93	7.02	1.235	0.052	-0.207	0.492
HD92074	8.64	G0	5842 ± 69	4.56 ± 0.08	0.070 ± 0.026	5,1,5,5,5	7.46	7.15	7.11	7.06	7.09	7.09	7.08	1.577	0.293	-0.182	1.150
HD93215	8.05	G5V	5558	4.09	0.040	1,1,2,2,2	6.89	6.60	6.55	6.48	6.52	6.56	6.54	0.725	1.623	-0.779	0.261
HD93489	7.92	G3V	5904	4.41	0.040	1,1,2,2,2	6.81	6.50	6.47	6.39	6.45	6.48	6.38	0.577	1.522	-0.530	1.101
HD98618	7.65	G5V	5838 ± 21	4.42 ± 0.03	-0.010 ± 0.020	5,1,5,5,5	6.45	6.14	6.06	5.97	5.99	6.05	5.99	0.355	1.818	-0.273	0.924
HD101364	8.67	G5	5795 ± 23	4.43 ± 0.03	0.023 ± 0.014	5,1,5,5,5	7.48	7.20	7.16	7.09	7.14	7.13	7.12	1.215	0.360	-0.320	0.857
HD101530	8.07	G2V	5839	4.41	-0.190	1,1,2,2,2	6.98	6.71	6.62	6.56	6.59	6.61	6.55	0.516	1.098	-0.415	0.320
HD102117	7.47	G6V	5690 ± 22.00	4.30 ± 0.04	0.304 ± 0.030	5,1,5,5,5	6.22	5.95	5.83	5.80	5.73	5.83	5.69	0.102	1.536	-0.395	0.836
HD107148	8.01	G5	5811 ± 21.00	4.38 ± 0.04	0.315 ± 0.030	5,1,5,5,5	6.86	6.60	6.47	6.46	6.47	6.50	6.41	0.076	0.971	-0.450	0.879
HD107633	8.78	G6V	5874 ± 72.00	4.52 ± 0.10	0.110 ± 0.033	5,1,5,5,5	7.59	7.33	7.29	7.21	7.24	7.24	7.28	2.68	0.345	-0.239	0.232
HD109573	5.78	A0V	10000	4.00	-0.030	1,1,12,12, 17	5.78	5.79	5.77	5.37	5.40	5.02	1.22	2.756	1.923	7.830	17.000
HD110668	8.29	G3G5V	5819	4.42	0.190	1,1,2,2,2	7.15	6.87	6.79	6.76	6.79	6.81	6.77	0.331	0.549	-0.302	0.547
HD113766	7.48	F3/F5V	7250	3.50	0.010	1,1,13,13,14	6.73	6.59	6.49	6.36	5.97	3.50	1.75	0.280	6.853	20.021	16.954
HD114826	8.92	G5	5860 ± 110	4.56 ± 0.11	0.120 ± 0.037	5,1,5,5,5	7.74	7.53	7.42	7.37	7.41	7.41	7.37	1.880	0.051	-0.182	0.143
HD115739	8.86	G3/G5V	5875 ± 30	4.56 ± 0.06	0.090 ± 0.030	5,1,5,5,5	7.72	7.40	7.34	7.31	7.35	7.36	7.16	1.523	0.024	-0.418	1.602

Star	V (mag)	ST (K)	T _{eff} (cm s ⁻²)	log g (dex)	[Fe/H]	Ref (mag)	J (mag)	H (mag)	K (mag)	[3.4] (mag)	[4.6] (mag)	[12] (mag)	[22]	X3.4	X4.6	X12	X22
HD119856	8.21	G1V	5894	4.58	-0.140	1,1,2,2,2	7.08	6.83	6.74	6.67	6.72	6.73	6.62	0.418	0.614	-0.367	1.519
HD122973	8.08	G0	5982	4.51	0.120	1,1,2,2,2	7.01	6.75	6.67	6.51	6.58	6.62	6.49	1.067	1.625	-0.489	0.299
HD123152	8.88	G2/G3V	5670 ± 30	4.31 ± 0.06	-0.450 ± 0.030	5,1,5,5,5	7.67	7.34	7.25	7.22	7.28	7.31	7.31	1.015	0.375	-0.728	-0.724
HD125612	8.31	G3V	5874	4.51	0.220	1,1,2,2,2	7.18	6.95	6.84	6.80	6.83	6.84	6.88	0.365	0.162	-0.159	0.400
HD134664	7.76	G2V	5884	4.43	0.130	1,1,2,2,2	6.60	6.32	6.25	6.18	6.24	6.27	6.15	0.595	1.032	-0.523	1.324
HD134902	8.85	G0	5853 ± 57	4.51 ± 0.08	0.090 ± 0.026	5,1,5,5,5	7.64	7.39	7.32	7.27	7.33	7.32	7.30	1.877	0.311	-0.471	0.506
HD138159	9.16	G2V	5775 ± 25	4.56 ± 0.05	-0.020 ± 0.020	5,1,5,5,5	7.98	7.70	7.63	7.57	7.61	7.60	7.55	0.526	0.023	-0.114	0.382
HD141937	7.25	G2/G3V	5900 ± 19	4.45 ± 0.04	0.125 ± 0.030	5,1,5,5,5	6.13	5.87	5.76	5.77	5.68	5.80	5.73	-4.369	1.676	-0.267	1.314
HD142072	7.85	G5V	5761	4.38	0.140	1,1,2,2,2	6.71	6.43	6.32	6.31	6.30	6.33	6.20	-0.075	0.891	-0.302	1.074
HD144270	8.21	F8	5923 ± 67	4.57 ± 0.08	0.000 ± 0.027	5,1,5,5,5	7.05	6.75	6.74	6.68	6.71	6.70	6.62	0.461	-0.215	-0.049	1.427
HD145478	8.67	G0	5945 ± 30	4.53 ± 0.06	0.110 ± 0.030	5,1,5,5,5	7.50	7.26	7.17	7.16	7.18	7.18	7.13	0.819	-0.010	-0.191	0.920
HD145518	7.41	G1/G2V	5900	4.49	-0.060	1,1,2,2,2	6.30	6.02	5.96	5.88	5.85	5.97	5.85	0.195	1.491	-0.405	0.889
HD146070	7.53	G1V	5821	4.43	-0.090	1,1,2,2,2	6.41	6.11	6.04	6.01	6.01	6.07	5.95	-0.065	1.008	-0.408	1.232
HD150027	8.99	G5/G6V	5640 ± 30	4.21 ± 0.06	-0.180 ± 0.030	5,1,5,5,5	7.75	7.47	7.43	7.33	7.39	7.38	7.26	1.118	-0.087	-0.113	1.501
HD152322	8.01	G3V	5949	4.57	0.020	1,1,2,2,2	6.90	6.65	6.58	6.52	6.57	6.58	6.57	0.148	0.372	-0.230	0.330
HD154221	8.60	G3V	5880 ± 30	4.45 ± 0.06	0.150 ± 0.030	5,1,5,5,5	7.45	7.17	7.10	7.00	7.02	7.09	7.06	1.735	0.145	-0.290	-0.425
HD155114	7.53	G3V	5791	4.56	-0.070	1,1,2,2,2	6.35	6.06	6.00	5.99	5.94	6.02	5.96	-0.273	1.365	-0.462	0.765
HD155968	8.41	G5	5720	4.47	0.160	1,1,2,2,2	7.23	6.95	6.87	6.86	6.86	6.88	6.87	0.111	0.189	-0.216	1.037
HD156922	9.10	G3V	5700 ± 30	4.42 ± 0.06	-0.340 ± 0.030	5,1,5,5,5	7.90	7.58	7.53	7.47	7.52	7.49	7.39	0.566	0.286	-0.252	0.581
HD157691	8.37	G3/G5V	5730 ± 30	4.43 ± 0.06	-0.390 ± 0.030	5,1,5,5,5	7.18	6.89	6.78	6.75	6.79	6.82	6.79	0.303	0.614	-0.497	1.033
HD165357	8.89	G3V	5835 ± 30	4.32 ± 0.06	0.070 ± 0.030	5,1,5,5,5	7.72	7.48	7.33	7.31	7.37	7.36	7.20	1.298	-0.140	-0.214	1.472
HD168746	7.95	G5	5572	4.44	-0.070	1,1,2,2,2	6.68	6.33	6.25	6.02	6.13	6.14	5.43	5.059	-0.050	-0.883	5.211
HD171918	7.98	G0	5775 ± 25	4.20 ± 0.05	0.206 ± 0.030	5,1,5,5,5	6.76	6.45	6.38	6.30	6.34	6.39	6.29	1.357	1.688	-2.526	-0.439
HD181296	5.03	A0Vn	9500	4.00	0.170	1,1,1,1,1,1,7	5.09	5.14	5.00	5.05	4.82	4.72	3.26	-2.521	-1.224	0.562	12.635
HD183505	8.16	G3IV/V	5716	4.52	0.140	1,1,2,2,2	6.98	6.67	6.59	6.51	6.59	6.61	6.51	0.294	0.557	-0.532	1.106

Star	V (mag)	ST	T _{eff} (K)	log g (cm s ⁻²)	[Fe/H] (dex)	Ref	J (mag)	H (mag)	K (mag)	[3.4] (mag)	[4.6] (mag)	[12] (mag)	[22] (mag)	χ _{3.4}	χ _{4.6}	χ ₁₂	χ ₂₂
HD192417	8.20	G3V	5745	4.56	0.050	1,1,2,2,2	6.98	6.75	6.60	6.57	6.57	6.63	6.55	0.272	0.791	-0.428	0.575
HD201422	8.54	G5V	5836 ± 48	4.50 ± 0.06	-0.160 ± 0.022	5,1,5,5,5	7.37	7.11	7.02	6.96	7.00	7.01	7.02	1.592	0.566	-0.588	0.082
HD207043	7.59	G5V	5731	4.46	0.030	1,1,2,2,2	6.42	6.10	6.05	6.02	5.98	6.04	5.98	-0.202	1.354	-0.315	1.029
HD209096	8.94	G5V	5875 ± 51	4.51 ± 0.07	0.150 ± 0.024	5,1,5,5,5	7.77	7.49	7.44	7.36	7.40	7.41	7.25	1.993	0.207	-0.518	1.244
HD209262	8.00	G5	5760	4.40	0.130	1,1,2,2,2	6.82	6.60	6.45	6.42	6.44	6.46	6.36	0.670	0.980	-0.497	1.259
HD213199	8.16	G2V	5908	4.41	-0.040	1,1,2,2,2	7.05	6.80	6.75	6.68	6.72	6.74	6.67	0.604	0.583	-0.286	1.211
HD214954	8.26	G3/G5IV	5727	4.50	0.180	1,1,2,2,2	7.12	6.81	6.70	6.67	6.68	6.69	6.67	0.138	0.543	-0.264	0.505
HD215657	7.22	G3IV-V	5989	4.42	0.070	1,1,2,2,2	6.13	5.87	5.78	5.73	5.66	5.79	5.75	-0.645	0.656	-1.217	0.017
HD218205	7.67	G2V	5945	4.55	0.120	1,1,2,2,2	6.54	6.29	6.20	6.17	6.19	6.24	6.24	0.225	2.819	-0.612	0.388
HD218396	5.96	A5V	7430 ± 75	4.35 ± 0.05	-0.470 ± 0.100	5,1,5,5,5	5.38	5.28	5.24	5.19	5.05	5.21	4.85	0.251	2.123	0.675	4.803
HD221343	8.37	G2V	5822	4.58	0.120	1,1,2,2,2	7.21	6.92	6.83	6.81	6.85	6.85	6.72	0.224	0.318	-0.371	1.217
HD222669	7.68	G2V	5877	4.46	0.090	1,1,2,2,2	6.58	6.26	6.24	6.21	6.18	6.21	6.15	-0.313	1.666	-0.432	0.741
HD224448	9.02	G0	5905 ± 44	4.55 ± 0.07	-0.010 ± 0.022	5,1,5,5,5	7.88	7.58	7.51	7.49	7.50	7.51	7.23	0.947	0.159	-0.206	0.923
HD225299	8.13	G5V	5754	4.56	0.230	1,1,2,2,2	6.88	6.65	6.50	6.51	6.55	6.55	6.56	-0.051	1.319	-0.441	0.732
HD238838	8.84	G5	5796 ± 73	4.48 ± 0.12	-0.020 ± 0.038	5,1,5,5,5	7.59	7.30	7.23	7.19	7.24	7.24	7.27	0.657	0.516	-0.338	-0.142
HIP2894	8.64	G0	5820 ± 44	4.54 ± 0.07	-0.030 ± 0.025	5,1,5,5,5	7.49	7.18	7.11	7.04	7.11	7.10	7.14	1.576	-0.016	-0.286	0.244
HIP8841	9.23	G5	5676 ± 45	4.50 ± 0.06	-0.120 ± 0.021	5,1,5,5,5	8.03	7.68	7.64	7.55	7.62	7.62	7.50	1.762	-0.375	-0.231	0.974
HIP49572	9.27	G0	5831 ± 52	4.33 ± 0.06	0.010 ± 0.021	5,1,5,5,5	8.06	7.80	7.73	7.65	7.68	7.69	7.60	1.688	-0.016	-0.436	0.569
HIP78028	9.23	G5	5790 ± 58	4.46 ± 0.07	-0.020 ± 0.025	5,1,5,5,5	8.03	7.73	7.67	7.60	7.64	7.63	7.97	0.595	-0.158	0.066	-0.699
HIP81512	8.63	G5	5879 ± 98	4.57 ± 0.12	-0.030 ± 0.041	5,1,5,5,5	7.44	7.16	7.09	7.07	7.12	7.11	7.12	0.326	0.265	-0.372	0.898
Twins																	
HD3821	7.02	G0	5850 ± 10	4.52 ± 0.02	-0.087 ± 0.008	6,1,6,6,6	5.91	5.60	5.52	5.53	5.29	5.55	5.470	0.082	1.889	-0.311	1.463
HD6204	8.52	G0	5854 ± 10	4.50 ± 0.02	0.028 ± 0.008	6,1,6,6,6	7.35	7.08	6.96	6.88	6.97	7.00	7.220	2.101	0.260	-0.282	-1.684
HD8291	8.61	G5	5764 ± 8	4.52 ± 0.01	-0.068 ± 0.007	6,1,6,6,6	7.42	7.14	7.07	6.98	7.02	7.04	6.920	0.954	-0.046	-0.231	1.251
HD11195	8.89	G5V	5725 ± 6	4.49 ± 0.02	-0.096 ± 0.006	6,1,6,6,6	7.67	7.37	7.27	7.19	7.22	7.23	7.110	2.552	-0.194	-0.239	1.154
HD13357	7.63	G5+	5738 ± 7	4.51 ± 0.01	-0.007 ± 0.005	6,1,6,6,6	6.91	6.66	6.58	6.56	6.58	6.63	6.510	0.253	0.700	-0.420	0.689

Star	V (mag)	ST	T_{eff} (K)	$\log g$ (cm s^{-2})	[Fe/H] (dex)	Ref	J (mag)	H (mag)	K (mag)	[3.4] (mag)	[4.6] (mag)	[12] (mag)	[22] (mag)	$\chi_{3.4}$	$\chi_{4.6}$	χ_{12}	χ_{22}
HD26990	7.50	G0	5764 ± 12	4.47 ± 0.04	-0.070 ± 0.011	6,1,6,6,6	6.25	5.95	5.85	5.84	5.76	5.87	5.760	-0.027	1.442	-0.382	0.620
HD28904	8.26	G5V	5846 ± 11	4.50 ± 0.03	-0.070 ± 0.008	6,1,6,6,6	7.00	6.69	6.58	6.48	6.51	6.50	6.410	0.067	0.458	-0.196	1.382
HD30774	7.88	G3/G5V	5789 ± 8	4.43 ± 0.02	0.084 ± 0.008	6,1,6,6,6	6.58	6.23	6.13	6.04	6.02	6.09	6.000	0.861	0.056	-0.236	1.456
HD35769	8.67	G5	5631	4.34	-0.130	1,1,2,2,2	7.41	7.08	7.04	7.03	7.05	7.05	7.150	0.225	2.054	-0.613	1.118
HD36152	8.27	G5V	5771 ± 5	4.44 ± 0.02	0.057 ± 0.005	6,1,6,6,6	7.08	6.87	6.73	6.80	6.82	6.81	6.830	0.659	-0.022	-0.307	1.397
HD39649	8.52	G5V	5740	4.40	0.010	3,19,2,2,2	7.37	7.05	6.99	6.93	6.98	6.98	6.830	0.497	-0.111	-0.197	1.497
HD41708	8.02	G0V	5928	4.45	0.080	1,1,2,2,2	6.88	6.63	6.58	6.54	6.53	6.58	6.440	-0.148	0.682	-0.938	1.430
HD44821	7.37	K0/1V(+G)	5750 ± 9	4.50 ± 0.02	0.063 ± 0.007	6,1,6,6,6	6.18	5.91	5.81	5.72	5.68	5.78	5.700	0.161	1.730	-0.230	1.364
HD45021	9.16	G5V	5668 ± 5	4.42 ± 0.01	-0.011 ± 0.004	6,1,6,6,6	7.95	7.68	7.59	7.48	7.54	7.53	7.570	-0.845	-0.102	0.035	0.276
HD45346	8.66	G5V	5721 ± 6	4.41 ± 0.02	-0.076 ± 0.006	6,1,6,6,6	7.47	7.14	7.07	7.04	7.07	7.08	7.110	0.341	0.127	-0.223	0.446
HD59711	7.73	G5V	5737 ± 4	4.41 ± 0.01	-0.117 ± 0.004	6,1,6,6,6	6.52	6.21	6.15	6.15	6.13	6.18	6.160	-0.136	1.798	-0.371	0.876
HD59967	6.66	G3V	5847 ± 12	4.54 ± 0.02	-0.021 ± 0.009	6,1,6,6,6	5.53	5.25	5.10	5.05	4.84	5.10	4.940	0.124	1.952	-0.418	2.033
HD63487	9.20	G2V	5849 ± 8	4.49 ± 0.02	0.058 ± 0.007	6,1,6,6,6	8.03	7.75	7.67	7.63	7.68	7.63	7.230	0.796	0.260	-0.426	1.092
HD67010	8.51	G5	5613	4.48	-0.130	1,1,2,2,2	7.30	6.96	6.86	6.79	6.85	6.87	6.870	0.771	0.238	-0.364	0.447
HD75302	7.45	G0	5702 ± 5	4.46 ± 0.01	0.083 ± 0.006	6,1,6,6,6	6.24	5.95	5.84	5.89	5.74	5.81	5.810	-2.542	-0.173	1.322	-0.256
HD78660	8.34	G5	5776	4.47 ± 0.02	-0.023 ± 0.005	6,1,6,6,6	7.11	6.89	6.76	6.74	6.79	6.78	6.650	0.266	0.158	-0.234	1.388
HD96116	8.65	G3V	5820 ± 9	4.51 ± 0.02	-0.014 ± 0.007	6,1,6,6,6	7.50	7.20	7.08	7.07	7.11	7.11	7.320	1.913	-0.191	-0.086	0.196
HD96423	7.23	G5V	5727 ± 4	4.36 ± 0.01	0.118 ± 0.004	6,1,6,6,6	6.02	5.74	5.63	5.70	5.49	5.65	5.610	-2.888	3.034	-0.548	0.471
HD97356	8.15	G5	5805	4.35	0.020	1,1,2,2,2	6.97	6.70	6.62	6.55	6.61	6.64	6.570	0.561	1.178	-0.535	1.005
HD98618	8.15	G5V	5805	4.35	0.020	1,1,2,2,2	6.97	6.70	6.62	6.55	6.61	6.64	6.570	0.561	1.178	-0.535	1.005
HD115169	9.26	G3V	5767 ± 8	4.46 ± 0.02	-0.067 ± 0.007	6,1,6,6,6	8.09	7.77	7.71	7.65	7.70	7.69	7.640	1.143	0.347	-0.510	0.342
HD122194	9.39	G3V	5845 ± 6	4.37 ± 0.02	0.054 ± 0.005	6,1,6,6,6	8.16	7.93	7.77	7.74	7.80	7.78	7.780	1.016	0.132	-0.234	1.088
HD129814	7.52	G5V	5842 ± 8	4.35 ± 0.02	-0.034 ± 0.007	6,1,6,6,6	6.33	6.07	6.00	5.93	5.90	5.98	5.910	0.234	1.221	-0.398	1.095
HD134664	7.76	G2V	5844 ± 5	4.49 ± 0.01	0.077 ± 0.004	6,1,6,6,6	6.60	6.32	6.25	6.18	6.24	6.27	6.150	0.595	1.032	-0.523	1.324
HD138573	7.22	G5IV-V	5777	4.46	-0.037 ± 0.006	6,1,6,6,6	6.03	5.74	5.66	5.61	5.53	5.68	5.620	0.119	2.563	-0.680	0.960
HD140538	5.86	G5V	5683 ± 5	4.48 ± 0.02	0.036 ± 0.006	6,1,6,6,6	4.59	4.05	4.30	4.13	3.55	4.17	4.140	-0.129	1.311	-0.450	0.597

Star	V (mag)	ST	T _{eff} (K)	log g (cm s ⁻²)	[Fe/H] (dex)	Ref	J (mag)	H (mag)	K (mag)	[3.4] (mag)	[4.6] (mag)	[12] (mag)	[22] (mag)	X3.4	X4.6	X12	X22
HD142331	8.72	G0	5690 ± 6	4.40 ± 0.02	-0.006 ± 0.006	6,1,6,6,6	7.48	7.18	7.13	7.09	7.12	7.13	7.130	0.976	-0.026	-0.096	0.451
HD142415	7.33	G1V	5904	4.40	0.080	1,1,2,2,2	6.24	5.99	5.89	5.83	5.80	5.90	5.840	-0.519	0.419	-1.382	-0.128
HD145927	8.35	G2III	5803 ± 6	4.38 ± 0.02	-0.041 ± 0.005	6,1,6,6,6	7.23	6.87	6.68	6.48	6.59	6.56	6.030	1.927	-0.164	0.228	2.148
HD147513	5.37	G3/G5V	5885	4.53	0.040	1,1,2,2,2	4.41	4.03	3.93	3.92	3.38	3.90	3.830	-0.076	1.138	-0.568	0.970
HD150248	7.03	G3V	5715 ± 5	4.40 ± 0.02	-0.086 ± 0.004	6,1,6,6,6	5.85	5.53	5.45	5.42	5.21	5.38	5.040	1.152	4.074	0.729	0.373
HD157347	6.28	G5IV	5694 ± 5	4.41 ± 0.02	0.015 ± 0.004	6,1,6,6,6	5.13	4.80	4.69	4.68	4.24	4.71	4.660	-0.558	0.964	-2.846	-0.851
HD163441	8.43	G5	5795	4.43	0.041 ± 0.006	6,1,6,6,6	7.17	6.83	6.76	6.66	6.74	6.73	6.590	0.312	0.331	-0.351	1.782
HD167060	8.93	G3V	5841 ± 5	4.44 ± 0.02	-0.037 ± 0.005	6,1,6,6,6	7.78	7.51	7.43	7.38	7.44	7.43	7.530	0.742	-0.023	-0.124	-0.345
HD173071	8.19	G0	6044	4.49	0.250	1,1,2,2,2	7.13	6.87	6.77	6.74	6.78	6.82	6.920	0.050	0.390	-0.445	0.492
HD183579	8.67	G5V	5781 ± 8	4.50 ± 0.02	-0.053 ± 0.007	6,1,6,6,6	7.52	7.23	7.15	7.09	7.13	7.11	7.060	0.800	0.219	-0.244	0.905
HD196390	7.33	G3V	5890 ± 6	4.47 ± 0.02	0.057 ± 0.006	6,1,6,6,6	6.21	5.95	5.87	5.81	5.78	5.87	5.790	-0.034	1.371	-0.270	1.168
HD197027	9.18	G3V	5718 ± 5	4.40 ± 0.02	-0.020 ± 0.005	6,1,6,6,6	7.96	7.68	7.59	7.55	7.59	7.61	7.920	1.185	-0.040	-0.247	-1.005
HD208704	7.16	G5/G6V	5829 ± 7	4.33 ± 0.02	-0.111 ± 0.006	6,1,6,6,6	6.03	5.72	5.66	5.59	5.58	5.67	5.620	-0.101	1.552	-0.546	0.850
HD209562	8.88	G3V	5847 ± 17	4.53 ± 0.03	0.064 ± 0.013	6,1,6,6,6	7.70	7.42	7.36	7.30	7.34	7.33	7.520	2.127	-0.064	-0.316	-0.256
HD209779	7.57	G0	5787 ± 17	4.50 ± 0.04	0.035 ± 0.014	6,1,6,6,6	6.33	6.00	5.88	5.87	5.74	5.86	5.810	-0.807	1.620	-0.419	0.854
HD219057	9.60	G3V	5816 ± 9	4.52 ± 0.02	-0.077 ± 0.008	6,1,6,6,6	8.46	8.19	8.09	8.03	8.07	8.08	8.700	0.964	-0.017	-0.176	-1.446
HD220507	7.59	G5V	5699 ± 9	4.25 ± 0.03	0.036 ± 0.008	6,1,6,6,6	6.38	6.10	5.97	5.88	5.90	6.00	5.970	0.803	1.427	-0.502	0.514
HD222582	7.68	G5	5792 ± 6	4.37 ± 0.02	0.010 ± 0.005	6,1,6,6,6	6.52	6.24	6.17	6.08	6.09	6.16	6.000	0.238	2.667	-0.416	1.158
Int1	12.86	...	5837 ± 11	4.42 ± 0.03	0.07 ± 0.01	18,7,7,7	11.56	11.25	11.17	11.14	11.20	11.00	...	1.850	0.955	0.131	...
MMJ5484	14.54	...	5768 ± 70	7,7	13.35	13.06	12.93	12.92	12.94	11.68	8.78	-3.267	-4.639	< 10.992	< 15.309
MMJ6055	14.56	...	5693 ± 74	7,7	13.34	13.02	12.95	12.93	12.98	12.05	9.01	-3.435	-3.455	< 12.112	< 15.277
MMJ6384	14.65	...	5756 ± 60	7,7	13.41	13.16	13.05	12.92	12.97	12.03	8.18	0.165	-0.084	< 6.165	< 15.443
S770	14.61	...	5766 ± 64	7,7	13.37	13.04	12.97	12.97	13.03	11.87	8.53	0.697	0.913	< 12.954	< 15.383
S779	14.64	...	5716 ± 64	7,7	13.40	13.04	12.96	13.00	13.01	11.72	8.67	1.929	0.967	< 11.096	< 15.430

Star	V (mag)	ST	T _{eff} (K)	log g (cm s ⁻²)	[Fe/H] (dex)	Ref	J (mag)	H (mag)	K (mag)	[3.4] (mag)	[4.6] (mag)	[12] (mag)	[22] (mag)	X3.4	X4.6	X12	X22
S785	14.81	...	5716 ± 63	7,7	13.53	13.20	13.07	13.11	13.15	12.25	8.93	7.849	6.021	< 11.252	< 13.939
S945	14.46	...	5836 ± 67	7,7	13.31	12.95	12.94	12.90	12.92	11.82	8.59	1.519	1.218	< 12.003	< 15.318
S966	14.49	...	5806 ± 65	7,7	13.27	13.00	12.95	12.86	12.90	11.37	8.22	2.791	1.296	3.831	< 4.462
S1041	14.73	...	5704 ± 64	7,7	13.34	12.99	12.90	12.86	12.96	12.43	8.84	8.279	7.411	< 7.494	< 15.561
S1462	14.29	...	5874 ± 58	7,7	13.03	12.67	12.60	12.58	12.61	12.38	8.85	-1.969	-2.447	< 9.416	< 15.135
Sibling candidates																	
HD10157	8.83	G0	6046	4.59	0.110	8,1,8,8,8	7.74	7.47	7.43	7.35	7.42	7.41	7.55	1.194	0.042	-0.116	-0.814
HD11124	8.76	F6V	6111	4.43	-0.100	8,1,8,8,8	7.82	7.57	7.50	7.38	7.48	7.47	7.32	1.764	0.240	-0.380	1.325
HD14706	8.71	G0V	5995	4.45	-0.070	8,1,8,8,8	7.60	7.33	7.20	7.07	7.16	7.16	7.03	1.887	0.197	-0.216	1.577
HD19573	7.62	G0	6461	4.13	-0.090	8,1,8,8,8	6.72	6.52	6.48	6.47	6.39	6.48	6.35	-0.067	1.565	-0.479	1.419
HD21216	8.44	F8	6184	4.39	-0.190	8,1,8,8,8	7.53	7.33	7.30	7.15	7.23	7.23	6.63	1.708	-0.272	-0.353	5.000
HD30059	9.31	G8/KV	5481	4.54	0.160	8,1,8,8,8	8.00	7.67	7.57	7.53	7.60	7.58	7.61	0.831	0.408	-0.324	5.033
HD33503	7.64	F8III	6531	4.20	0.030	8,1,8,8,8	6.78	6.56	6.52	6.53	6.47	6.55	6.47	-0.161	1.186	-0.460	5.943
HD35874	8.19	F6V	6526	4.23	0.240	8,1,8,8,8	7.25	7.12	7.02	6.97	6.99	7.00	6.96	0.673	0.016	-0.157	0.865
HD37574	6.74	F8	6344	3.90	-0.050	8,1,8,8,8	5.79	5.59	5.54	5.55	5.47	5.66	5.55	0.141	1.660	-1.074	1.268
HD44821	7.37	K0/1V(+G)	5744	4.59	0.070	8,1,8,8,8	6.18	5.91	5.81	5.76	5.67	5.78	5.69	0.161	1.730	-0.230	1.364
HD50867	7.60	F8	6218	4.32	-0.090	8,1,8,8,8	6.65	6.45	6.33	6.35	6.28	6.36	6.33	-0.213	1.251	-0.415	0.363
HD52242	7.39	F2/F3V	6752	4.23	-0.060	8,1,8,8,8	6.61	6.46	6.39	6.38	6.32	6.39	6.29	-0.119	1.129	-0.398	1.142
HD84843	8.58	F8	6264	4.34	-0.160	8,1,8,8,8	7.62	7.48	7.39	7.25	7.36	7.35	7.32	2.316	-0.351	-0.046	0.519
HD91320	8.43	G1V	5981	4.13	-0.050	8,1,8,8,8	7.34	7.12	7.01	6.89	7.00	7.02	7.00	1.773	0.280	-0.342	0.337
HD95915	7.25	F6V	6305	4.04	-0.140	8,1,8,8,8	6.32	6.06	6.00	6.06	5.93	6.02	5.94	-1.194	1.565	-0.515	0.970
HD101197	8.73	G5	5672	4.19	0.000	8,1,8,8,8	7.57	7.30	7.21	7.02	7.20	7.18	7.19	2.941	0.541	-0.567	0.083
HD105000	7.91	F2	6509	4.32	0.010	8,1,8,8,8	7.09	6.91	6.82	6.79	6.79	6.84	6.89	0.343	0.757	-0.388	-0.297
HD105678	6.34	F6IV	6166	3.66	-0.100	8,1,8,8,8	5.42	5.17	5.10	5.09	4.89	5.12	5.07	0.117	2.872	-0.331	0.782
HD108271	8.31	F8	6101	4.03	-0.240	8,1,8,8,8	7.30	7.12	7.05	6.97	7.05	7.04	7.17	1.164	-0.297	-0.015	-0.829
HD133815	9.06	G5	5985	4.43	0.100	8,1,8,8,8	7.94	7.70	7.64	7.53	7.63	7.60	7.67	1.629	-0.150	-0.272	-0.349

Star	V (mag)	ST	T_{eff} (K)	$\log g$ (cm s^{-2})	[Fe/H] (dex)	Ref	J (mag)	H (mag)	K (mag)	[3-4] (mag)	[4,6] (mag)	[12] (mag)	[22] (mag)	X3.4	X4.6	X12	X22
HD168325	9.66	F8	3925	5.37	-0.030	8,1,8,8,8	7.08	6.46	6.28	6.20	6.16	6.20	6.13	-0.042	1.826	-1.128	0.506
HD168442	7.49	K7V	6809	4.12	0.140	8,1,8,8,8	6.68	6.53	6.44	6.42	6.42	6.48	6.61	0.526	0.980	-0.273	-1.243
HD176118	8.24	F8	6321	4.19	-0.350	8,1,8,8,8	7.42	7.28	7.22	7.19	7.20	7.21	7.20	0.222	-0.179	-0.071	0.393
HD193549	6.46	F2IV/V	4828	3.23	-0.020	8,1,8,8,8	4.98	4.27	4.05	4.05	3.79	4.05	4.01	0.499	1.187	-0.050	0.060
HD196676	7.54	K0	6669	4.18	0.010	8,1,8,8,8	6.75	6.63	6.56	6.51	6.47	6.55	6.49	0.312	1.411	-0.419	0.879
HD207164	8.04	F2	5808	4.12	0.080	8,1,8,8,8	6.87	6.61	6.53	6.46	6.48	6.54	6.45	0.775	1.063	-0.460	1.140
HD219828	9.12	G0IV	5934	4.65	-0.040	8,1,8,8,8	7.90	7.68	7.58	7.48	7.52	7.52	7.48	1.167	0.151	-0.135	0.659
HIP76300	9.00	G5	6000	4.34	-0.110	8,1,8,8,8	7.80	7.52	7.46	7.33	7.33	7.34	6.74	1.139	0.547	-0.035	4.493
HIP112584	9.93	G0	5685	4.65	0.180	8,1,8,8,8	8.67	8.38	8.31	8.24	8.30	8.27	8.20	0.597	0.185	-0.381	0.532
Siblings																	
HD68314	8.76	A2/5II/III	6111	4.43	-0.100	1,19,8,8,8	7.82	7.57	7.50	7.38	7.48	7.47	7.32	1.764	0.240	-0.380	1.325
HD28676	8.71	F5	5995	4.45	-0.070	1,1,16,16,16	7.60	7.33	7.20	7.07	7.16	7.16	7.03	1.887	0.197	-0.216	1.577
HD83423	7.62	F8V	6461	4.13	-0.090	1,1,16,16,16	6.72	6.52	6.48	6.47	6.39	6.48	6.35	-0.067	1.565	-0.479	1.419
HD162826	8.83	F8V	6046	4.59	0.110	1,1,6,6,6	7.74	7.47	7.43	7.35	7.42	7.41	7.55	1.194	0.042	-0.116	-0.814
HD175840	9.31	K2	5481	4.54	0.160	1,1,16,16,16	8.00	7.67	7.57	7.53	7.60	7.58	7.61	0.831	0.408	-0.324	-0.033
HD186302	7.64	G3/G5V	6531	4.20	0.030	1,16,16,16	6.78	6.56	6.52	6.53	6.47	6.55	6.47	-0.161	1.186	-0.460	0.943

Notes. The references to the V magnitude, spectral type, effective temperature, surface gravity and metallicity are indicated by the numbers in column 7: (1) Hipparcos (ESA 1997); (2) Datzon et al. (2015); (3) Hog et al. (2000); (4) Houk & Swift (1999) (5) Ramirez et al. (2012); (6) Ramirez et al. (2014); (7) Pasquini et al. (2008); (8) Liu et al. (2015); (9) Ducati (2002); (10) Gray et al. (2006); (11) Chen et al. (2014); (12) Stauffer et al (1995); (13) Chen et al. (2011); (14) Nordström et al. (2004); (15) Chen et al. (2006); (16) Batista et al. (2014); (17) Saffe et al. (2008); (18) Henden et al (2016); (19) Houk & Smith-Moore (1998).